Coefficient of friction random field modelling and analysis in planar sliding

Han Hu[a], Anas Batou[b,*], Huajiang Ouyang[a]

[a] *Department of Mechanical, Materials and Aerospace Engineering, School of Engineering, University of Liverpool, Liverpool L69 7ZF, United Kingdom*
[b] *MSME, Univ Gustave Eiffel, CNRS UMR 8208, Univ Paris Est Creteil, F-77474 Marne-la-Vallée, France*

Abstract

In this paper, we investigate inherent mesoscale spatial fluctuations of the coefficient of friction (COF) in dry frictional phenomena by modelling it as a random field. The statistical properties of the resulting global random forces and torque are derived for three types of interface motion: pure translation, pure rotation and general planar motion. Closed-form formulas are derived for the case where the interface has a square geometry and a numerical simulation method is developed for more complex shapes. The analysis of these results shows that the statistical properties of the global forces and torque are functions of the ratio of the correlation length of the random field to the characteristic length of the interface, which enables limit analyses to be performed with respect to this ratio. These analyses provide guidance regarding whether the coefficient of friction should be modelled as a random field, a random variable or a deterministic variable. The concepts developed in this paper are illustrated through a simple crank-slider model for which the statistics of energy dissipated (because of the friction) are analysed concerning the value of the ratio of the correlation length to the sliding surface size.

Keywords: dry friction, random field, coefficient of friction, correlation length

1. Introduction

Dry friction plays a crucial role in widespread industrial applications. For example, dry friction accounts for the functional effectiveness in brake systems, wiper systems, musical instruments such as violin. On the other side, it is also the cause of undesirable oscillations in many mechanical systems that leads to consequences such as precision loss and control failure. To get a deep understanding of the mechanism of frictional phenomena, many researchers have devoted plenty of efforts on friction modelling for centuries since the pioneering work done by Da Vinci. As a result, various dry friction models have been proposed, from simple one like Coulomb's law to a much-complicated one including stick-slip effect like the LuGre model. For an extensive literature review, we refer to [1].

Dry friction is known to possess inherent randomness and have a significant influence on the system performance [2]. Besides, coefficients of friction (COF) exhibit strong dispersions with experimental proof [3,

*Corresponding author
Email address: batoua@liverpool.ac.uk (Anas Batou)

4, 5], whereas it is not until recent years that researches emerge on modelling friction in a stochastic approach. In general, random friction modelling involves treating COF as random variables [6, 7, 8, 9, 10, 11, 12, 13], a stochastic process [14, 15] or a random field [10, 16, 17, 18, 19] in the literature. For modelling COF as a random variable, Antonio et al.[6] studied the occurrence of squeal instability of a brake system, modelling the COF as random variables with the lognormal distribution. Lima et al.[7] investigated the dynamics of a block sliding on an inclined plane with friction modelled as a random function of position. Sarrouy et al.[8] investigated the brake squeal noise problem by modelling its COF as random parameters. A spatially uniform-like probability distribution was used to model the randomness of the COF and it outperformed the truncated Gaussian law on predicting the unstable modes and frequencies. Nechak et al.[9] proposed the Multi-Element Legendre Polynomial Chaos Method in dealing with the prediction of long time self friction-induced vibrations, and the friction coefficient involved was modelled as a uniform random variable. Kang et al.[11] performed a stochastic analysis of a mechanical system by characterizing the frictional parameters using experimental statistical data. Nobari et al.[12] investigated the mode-coupling instability in brake systems by conducting complex eigenvalue analysis. It was found that the COF was one of the most active parameters in the sensitivity analysis. Then the perturbation method was used by attributing a deviation of 15% to the COF concerning a normal distribution to perform an uncertainty analysis. Cherif Snoun et al.[13] developed a Multi-Element generalised Polynomial Chaos method to predict the discontinuity observed in the evolution of the Limit Cycle Oscillation of a 2-dof friction system. The COF was treated as one of the uncertain parameters and randomising its value through a given interval.

For modelling COF as a stochastic process, Choi et al.[14] modelled the uncertainty effects in the COF as a stationary truncated Gaussian process. The random friction was introduced in the model of a chain of Iwan oscillators to study the occurrence of stick and slip. Qiao et al.[15] analysed the dynamics of a disc brake under random COF modelled as a stochastic process. The probabilistic properties of transverse and circumferential displacements were derived and were found to be non-Gaussian, non-stationary, and narrowband processes. For modelling COF as a random field, Ritto et al.[10] studied the dynamics of a horizontal drill-string, and they modelled the frictional contact between the column and the borehole by representing the frictional coefficient as a stationary truncated Gaussian random field with exponential autocorrelation function. Gravanis et al.[16] performed a one-dimensional stability assessment of rock slopes through treating both COF and cohesion coefficient as Gaussian random fields, by which the probability of failure can be determined. And the work is extended to two-dimensional by Huang et al.[18] More generally, the randomness in friction also can be introduced through other ways. Kireenkov and Ramodanov [20] proposed a model of combined dry friction, in which the normal stresses within the contact spot was modelled as a time-depend random function thus resulted in random friction. Wierzcholski et al.[21] derived the statistical properties of random friction in the spherical human hip joint, in which the uncertainty was induced by the random changes of the joint gap height between the cartilage superficial layer and movable phospholipid bilayer. A similar stochastic analysis was applied to the frictional microbearing problem by

Wierzcholski and Miszczak [22] The random friction forces were caused by the random gap height between two rough surfaces in a computer micro bearing fan and computer microbearing in a hard disc drive.

In this paper, we pay particular attention to the planar sliding of a rigid body for which the spatially fluctuating friction coefficient field is modelled as a lognormal random field. Previous theoretical investigations of a similar problem using a deterministic approach can be found in the literature, see for instance [23, 24]. The frictional planar sliding problem also drives researches in various application scenarios, such as trajectory control in robotics [25, 26], dynamics of tippe top [27, 28] and the motion of rattleback [29] and billiard ball [30]. However, few papers have addressed the planar sliding problem in a stochastic framework. In general, the friction forces can be modelled by deterministic friction laws when the inherent spatial random fluctuations only appear at the micro-scale (asperities scale) and have little impact on the macro-scale dynamic of the rigid body. However, in some cases, the contact interfaces have a second scale of heterogeneities (see Fig.1) mainly due to the surface roughness and the spatial variations of material properties. For instance, in the automotive industry, the contact field of an automotive brake pad sample shows a large variability due to the surface roughness which yields the fluctuations in the friction forces, see Fig.3 in [31]. At this mesoscopic heterogeneities scale, even if the randomness induced by asperities becomes negligible, the roughness leads to random global forces and torques, thus demonstrating the necessity of the stochastic modelling of the COF. The objective of this paper is to analyse how the parameters of the random field and the contact surface affect the statistical properties of the random global friction force and torque, and to determine when it is worthwhile to take into account the computational cost this randomness. In such a random field modelling of the COF, contrary to deterministic modelling of dry friction, the global frictional force will depend on the size of the interface surface.

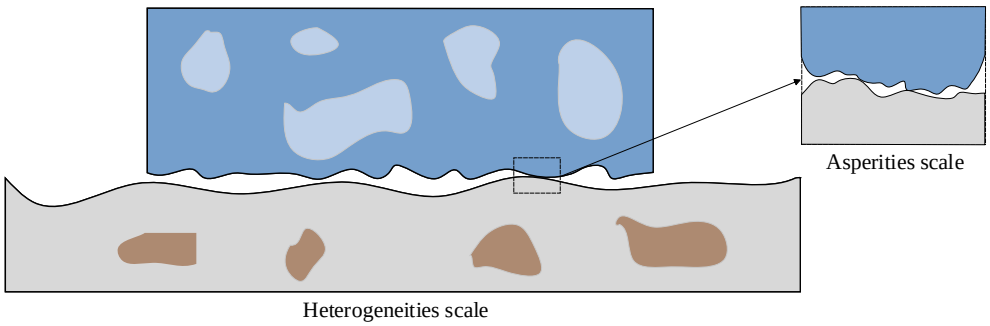

Fig. 1. Double-scale heterogeneities.

The remainder of this paper is organised as follows. In Sec.2 we derive the theoretical formulation of the planar sliding problem with random friction in pure translation, pure rotation and general planar motion condition. Limit analyses of the statistical properties of the global forces and the torque and numerical simulation are also performed. An application on a simple crank-slider model is introduced in Sec.3, in which we investigate the impact of the parameters of the random field modelling of the COF on the system

energy dissipation.

2. Theoretical formulations and numerical validation

In this section, we investigate a rigid square plate with a rough surface sliding on an infinite rigid flat plane under three particular conditions, namely pure translation, pure rotation and general planar motion, as shown in Fig.2. The purpose for the study of the former two conditions is to show that contrary to the deterministic modelling of uniform COF case, a random torque would be generated in the pure transitional motion and random frictional forces would be generated in the pure rotational motion when the COF is modelled as a random field. After that, a general planar motion case, which is a combination of the former two conditions, is investigated to provide more practical results.

The COF field of the sliding interface (denoted by Ω_S) present spatial random fluctuations and are then modelled by a homogeneous lognormal random field $\{\mathbb{H}(\mathbf{x}), \mathbf{x} \in \Omega_S\}$ where $\mathbf{x} = (x, y)$ is the vector of the interface surface 2D-coordinates in the body-fixed frame for which the origin is the geometric centre G of the interface (see Fig.2). The reasons for the chosen lognormal distribution are (1) it has an almost bell shape as the normal distribution; (2) it is positive in nature, which makes it suitable for representing COF. It should be noted that an early specification of the COF distribution is mainly for the convenience of numerical simulation. Other distributions, e.g. truncated Gaussian distribution, would also be applicable and not invalidate the conclusions of this paper. Furthermore, the correlation function $\{\mathrm{R}_{\mathbb{H}}(\mathbf{x}, \mathbf{x}'), (\mathbf{x}, \mathbf{x}') \in \Omega_S^2\}$ of the random field is assumed to be of Gaussian type and is then written as

$$\mathrm{R}_{\mathbb{H}}(\mathbf{x}, \mathbf{x}') = \mathrm{e}^{-\frac{\|\mathbf{x}-\mathbf{x}'\|^2}{l^2}} \ , \tag{1}$$

where l is the correlation length. It should be noted that the exact correlation length l_c is defined by $l_c = l\sqrt{\pi}/2$. However, in the remainder of the paper, only l will be used and will be referred to as the correlation length. Since the random COF field $\mathbb{H}(\mathbf{x})$ is assumed to be homogeneous, the marginal probability distribution function (pdf) is independent of $\mathbf{x}$ and can be expressed, for any $\mathbf{x} \in \Omega_S$, as:

$$p(h) = \frac{1}{h\sigma_h\sqrt{2\pi}}\mathrm{e}^{-(\ln(h)-m_h)^2/2\sigma_h^2} \ , \tag{2}$$

where

$$\begin{aligned} m_h &= \ln(\mu_{\mathbb{H}}) - \frac{1}{2}\ln(1+\frac{\sigma_{\mathbb{H}}^2}{\mu_{\mathbb{H}}^2}) \\ \sigma_h &= \sqrt{\ln(1+\frac{\sigma_{\mathbb{H}}^2}{\mu_{\mathbb{H}}^2})} \\ \mu_{\mathbb{H}} &= \mathbb{E}[\mathbb{H}(\mathbf{x})] \\ \sigma_{\mathbb{H}}^2 &= \mathbb{V}ar[\mathbb{H}(\mathbf{x})], \end{aligned} \tag{3}$$

where $\mathbb{E}[.]$ is the mathematical expectation and $\mathbb{V}ar[.]$ is the variance. As the plate moves on the plane, random friction forces (in the two surface directions) and a random torque (normal to the surface) will

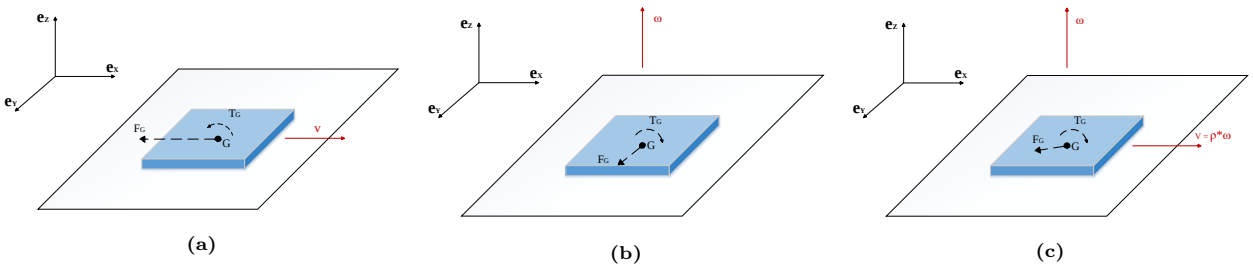

Fig. 2. Problem setting. (a) Pure translation case; (b) pure rotation case; (c) general planar motion case.

be generated because of the random distribution of COF on the interface. The objective of the next two subsections is to derive and study the statistical properties of these random forces and torque.

2.1. Pure translation case

2.1.1. Theoretical formulation

In pure translation motion, we assume that the square plate has an instant velocity $\mathbf{v}$ in the $\mathbf{e_x}$ direction only as shown in Fig.2a for the convenient presentation of result. Then, assuming a local Coulomb's friction model, the global generated friction force and global torque (at G) at the centre of mass can be expressed as

$$\mathbf{F_G} = -\frac{\mathbf{v}}{|\mathbf{v}|}\iint_S P\,\mathbb{H}(\mathbf{x})\,\mathrm{d}S = -\iint_S P\,\mathbb{H}(\mathbf{x})\,\mathrm{d}S\,\mathbf{e_x} \tag{4}$$

$$\mathbf{T_G} = -\iint_S P\,\mathbb{H}(\mathbf{x})\,\mathbf{x}\,\mathrm{d}S \times \frac{\mathbf{v}}{|\mathbf{v}|} = -\iint_S P\,\mathbb{H}(\mathbf{x})\,y\,\mathrm{d}S\,\mathbf{e_z}\ , \tag{5}$$

where $\times$ denotes the mathematical cross product and P is a constant scaling factor equal to the mean value of the pressure and not the local pressure. The friction force and torque can be decomposed as $\mathbf{F_G} = F_x\,\mathbf{e_x} + F_y\,\mathbf{e_y}$ and $\mathbf{T_G} = T_G\,\mathbf{e_z}$, where $\mathbf{e_x}$, $\mathbf{e_y}$ and $\mathbf{e_z}$ are respectively the basis vectors in the x, y and z directions of a body-fixed frame with the origin being the centre of mass of the plate as shown in Fig.2. In this case, $F_x = -\iint_S P\,\mathbb{H}(\mathbf{x})\,\mathrm{d}S$ and F_y is zero almost surely.

Remark 1. *We recognise that the contact pressure is not uniform when there is roughness. However, the product of $P\,\mathbb{H}(\mathbf{x})$ together makes the friction force and the torque random. In this study, we take an averaging P over the whole interface to justify the random field modelling of the COF.*

Remark 2. *It is important to note that an important feature of the classical deterministic Coulomb's friction model is that for a translational motion, no torque will be generated and the generated force is independent of the contact surface. In our case, a random torque is generated and both the random torque and the random force depend on the surface through the random distribution of the coefficient of friction over the contact surface.*

2.1.2. Derivation of the statistical properties of the random friction force and torque

Here, the statistical properties of the friction force and torque are derived. For computational simplicity, we assume that the geometry of the plate is a square, i.e., $\mathbf{x} \in [-a, a]^2$, where a is half length of the square plate, which is also treated as the characteristic length of the plate. Since the objective is to perform a limit analysis regarding the size of the surface, this assumption will not impact the conclusions that will be formulated later. Thus, the first and second moment of the x-component of the friction force can be derived as

$$\mathbb{E}[F_x] = \mu_F = -\mu_{\mathbb{H}} \iint_S P \, \mathrm{d}S \; = \; -4P \, a^2 \mu_{\mathbb{H}} \tag{6}$$

$$\begin{aligned} \mathbb{V}ar[F_x] = \sigma_F^2 &= \mathbb{E}[(F_x - \mathbb{E}[F_x]) \cdot (F_x - \mathbb{E}[F_x])] \\ &= P^2 \iint_{S'} \iint_S \mathrm{C}_{\mathbb{H}}(\mathbf{x}, \mathbf{x}') \, \mathrm{d}S \mathrm{d}S' \\ &= P^2 \sigma_{\mathbb{H}}^2 \Big\{ 4\pi \mathrm{erf}^2(\frac{2a}{l}) a^2 l^2 + 4\sqrt{\pi} \mathrm{erf}(\frac{2a}{l})(\mathrm{e}^{-\frac{4a^2}{l^2}} - 1) a l^3 \\ &+ (1 - 2\mathrm{e}^{-\frac{4a^2}{l^2}} + \mathrm{e}^{-\frac{8a^2}{l^2}}) l^4 \Big\} \, , \end{aligned} \tag{7}$$

where $\mathrm{C}_{\mathbb{H}}(\mathbf{x}, \mathbf{x}') = \sigma_{\mathbb{H}}^2 \mathrm{R}_{\mathbb{H}}(\mathbf{x}, \mathbf{x}')$ is the covariance function between $\mathbb{H}(\mathbf{x})$ and $\mathbb{H}(\mathbf{x}')$, and $\sigma_{\mathbb{H}}^2 = \mathrm{C}_{\mathbb{H}}(\mathbf{0}, \mathbf{0})$, while $\mathrm{erf}(\tau) = \frac{1}{\sqrt{\pi}} \int_{-\tau}^{\tau} \mathrm{e}^{-t^2} \mathrm{d}t$ is the Gauss error function[32]. In a similar way, the first two moments of the torque can be derived as:

$$\mathbb{E}[T_G] = \mu_T = -\mu_{\mathbb{H}} \iint_S P y \mathrm{d}S = 0 \tag{8}$$

$$\begin{aligned} \mathbb{V}ar[T_G] = \sigma_T^2 &= \mathbb{E}[P^2 (\iint_S \mathbb{H}(\mathbf{x}) \, y \, \mathrm{d}S) \cdot (\iint_{S'} \mathbb{H}(\mathbf{x}') \, y' \, \mathrm{d}S')] \\ &= P^2 \iint_{S'} \iint_S (\mathrm{C}_{\mathbb{H}}(\mathbf{x}, \mathbf{x}') + \mu_{\mathbb{H}}^2) \, y \, y' \, \mathrm{d}S \mathrm{d}S' \\ &= P^2 \sigma_{\mathbb{H}}^2 \Big\{ \frac{4\pi}{3} \mathrm{erf}^2(\frac{2a}{l}) a^4 l^2 + \frac{4\sqrt{\pi}}{3} \mathrm{erf}(\frac{2a}{l})(\mathrm{e}^{-\frac{4a^2}{l^2}} - 2) a^3 l^3 \\ &+ (1 - \frac{4}{3}\mathrm{e}^{-\frac{4a^2}{l^2}} + \frac{1}{3}\mathrm{e}^{-\frac{8a^2}{l^2}}) a^2 l^4 + \frac{\sqrt{\pi}}{3} \mathrm{erf}(\frac{2a}{l})(1 - \mathrm{e}^{-\frac{4a^2}{l^2}}) a l^5 \\ &+ (\frac{1}{3}\mathrm{e}^{-\frac{4a^2}{l^2}} - \frac{1}{6}\mathrm{e}^{-\frac{8a^2}{l^2}} - \frac{1}{6}) l^6 \Big\}. \end{aligned} \tag{9}$$

It can easily be shown that the random friction force (x-component) and the random torque are uncorrelated as:

$$\begin{aligned} \mathrm{Cov}[T_G, F_x] &= \mathbb{E}[(T_G - \mathbb{E}[T_G]) \cdot (F_x - \mathbb{E}[F_x])] \\ &= P^2 \iint_{S'} \iint_S \mathbb{E}[\mathbb{H}(\mathbf{x}) \mathbb{H}(\mathbf{x}')] \, y \, \mathrm{d}S \mathrm{d}S' \\ &= 0. \end{aligned} \tag{10}$$

A complete approximate construction of the probability distribution of the random variables F_x and T_G can be found in Appendix A.

2.1.3. Numerical simulation, validation and analysis

The formulas derived hereinbefore are valid for a square interface. For a general interface geometry, the mean values and the variances can be estimated numerically. Below, this numerical approach is explained and validated for the square geometry for which closed-form formulas have been derived.

The interface between the plate and the plane is discretised by three-node triangular elements to represent patches in contact in H-scale. And the COF of each patch act as random variables in the random field. Practically, the random field is evaluated at node points and then midpoint method or spatial average method[33] can be applied to determine the COF for each patch. A general way to achieve this evaluation is by using Matrix Decomposition Method[34] with a Nataf transform of a normalised Gaussian random field. Then the Gaussian random field with N nodes can be represented by a random vector $\hat{\Psi}$, with values in $\mathbb{R}^N$, such that

$$\big(\hat{\Psi} - \mu\big)/\sigma \sim \mathcal{N}(0, \mathbf{\Sigma}) \ , \tag{11}$$

where μ and σ are the mean and standard deviation of the Gaussian distribution, and $\mathbf{\Sigma}$ is the $N \times N$ covariance matrix with components evaluated from specified correlation function (Eq.1) represented as:

$$\Sigma_{ij} = \sigma^2_{\mathbb{H}} \mathrm{R}_{\mathbb{H}}(\mathbf{x}_i, \mathbf{x}_j) \ , \tag{12}$$

where $\mathbf{x}_i$, $\mathbf{x}_j$ are the coordinates of the ith and jth nodes respectively. The covariance matrix is usually symmetric positive-definite, while in some cases it can be semi positive-definite and can be made positive-definite by introducing a small regularisation term to the diagonal elements [35]. Therefore, it has Cholesky decomposition as $\mathbf{\Sigma} = U^{\mathrm{T}}U$. And the random variables at node points can be evaluated as

$$\hat{\Psi} = \mu + \sigma U^{\mathrm{T}} \xi \ , \tag{13}$$

where ξ is an N-variate independent and identically distribution standard Gaussian random variable. To generate a lognormal random field, we take the Nataf transformation of the Gaussian random field as $\hat{\mathbb{H}} = \mathrm{F}^{-1}[\Phi(\xi)] = e^{\hat{\Psi}}$, where $\Phi(\cdot)$ is the cumulative distribution function (CDF) of the standard normal variable, $\mathrm{F}^{-1}(\cdot)$ is the inverse CDF of the lognormal random variable with specified mean $\mu_{\mathbb{H}}$ and std $\sigma_{\mathbb{H}}$, and $\hat{\mathbb{H}}$ is a discretised representation of the random field $\mathbb{H}(\mathbf{x})$. The final step is to perform a spatial averaging inside each element to determine the friction coefficient in H-scale.

Remark 3. *We note that the employment of Nataf transformation to the generated Gaussian random field will cause deviation of the covariance matrix* $\mathbf{\Sigma}$*. However, it has been shown in [36] that this distortion is small and would not change the effect of the correlation function.*

To validate the numerical estimation method on a square interface (for which closed-form formulas have been derived), we use the following parameters: $a \in [0.5, 2.5]$, $l \in [0.1, 1]$, $\mu_{\mathbb{H}} = 0.5$, $\sigma^2_{\mathbb{H}} = 0.01$, and $P = 1$. The mesh size of the field should be less than the correlation length and the characteristic length for capturing essential information in the field. In this work, we set mesh size as $h = \min(l, 0.1a)$. We note that as long

as the mesh size is small enough to be covered by the correlation length, a further refinement of the mesh is not necessary due to the ensemble averaging effect that many samples are to be realised and averaged, which in turn eliminates the significance of the mesh size effect. Two realisations of the COF random field are shown in Fig.3. Both the variances of the friction and torque are estimated using $N_s = 5000$ realisations, the

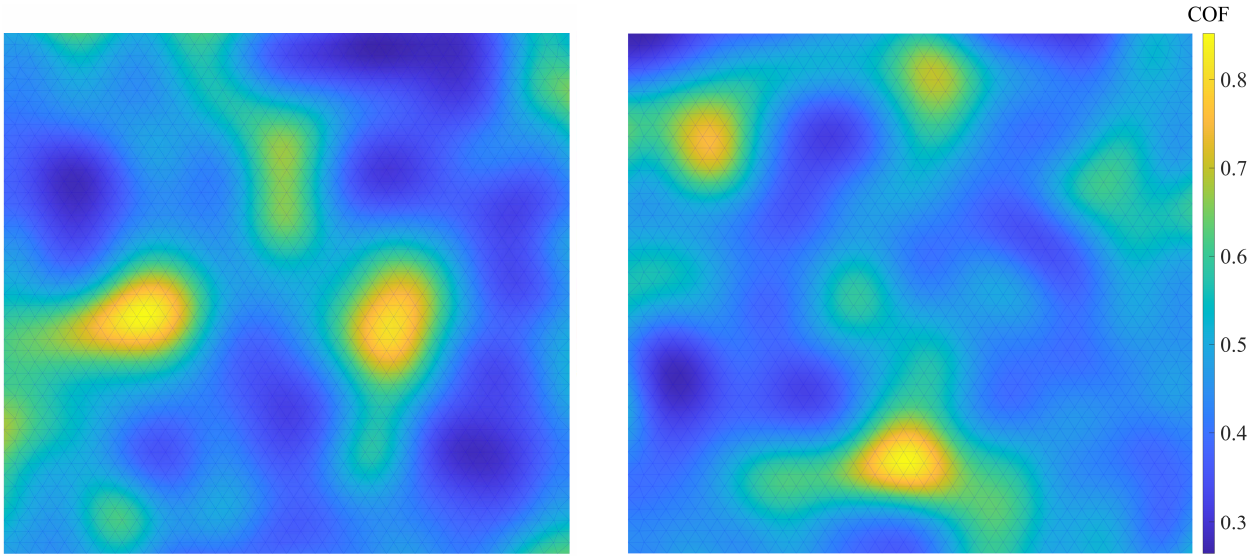

Fig. 3. Two realisations of COF random field.

estimated numerical and analytical solutions and relative error are illustrated in Fig.4 and Fig.5 for multiple values of the correlation length l and the size a of the surface. These results show that the variances of the friction force and torque show a similar trend with respect to the correlation length of the random field and the characteristic length of the contact interface, which is that they increase as l and a increase. And the trend becomes more evident when l and a grow proportionally.

The ensemble averaging effect is investigated through the relative error of F_x and T_G between analytical and numerical solutions in the case of $a = 1$ and $l = 1$ with sample size N_s, as depicted in Fig.6. The relative error declines dramatically as the sample size grows, although fluctuations emerge locally. Based on the results, herein and in the following, we use the sample size $N_s = 5000$ to ensure a low error.

2.1.4. Coefficient of variation of the friction force and torque

A more intuitive and informative way to analyse the inherent statistical properties of the random force and torque is to introduce dimensionless variables. Therefore, coefficient of variation (CV) is introduced for this purpose. CV is defined mathematically as the ratio of the standard deviation of the variable to its absolute mean value. Thus, we define $\mathrm{CV}_{\|\mathbf{F}\|}$ and CV_{T} as:

$$\mathrm{CV}_{\|\mathbf{F}\|} = \frac{\sigma_{\|\mathbf{F}\|}}{|\mu_{\|\mathbf{F}\|}|}, \tag{14}$$

$$\mathrm{CV}_{\mathrm{T}} = \frac{\sigma_T}{|\mu_{\|\mathbf{F}\|}| a_m}. \tag{15}$$

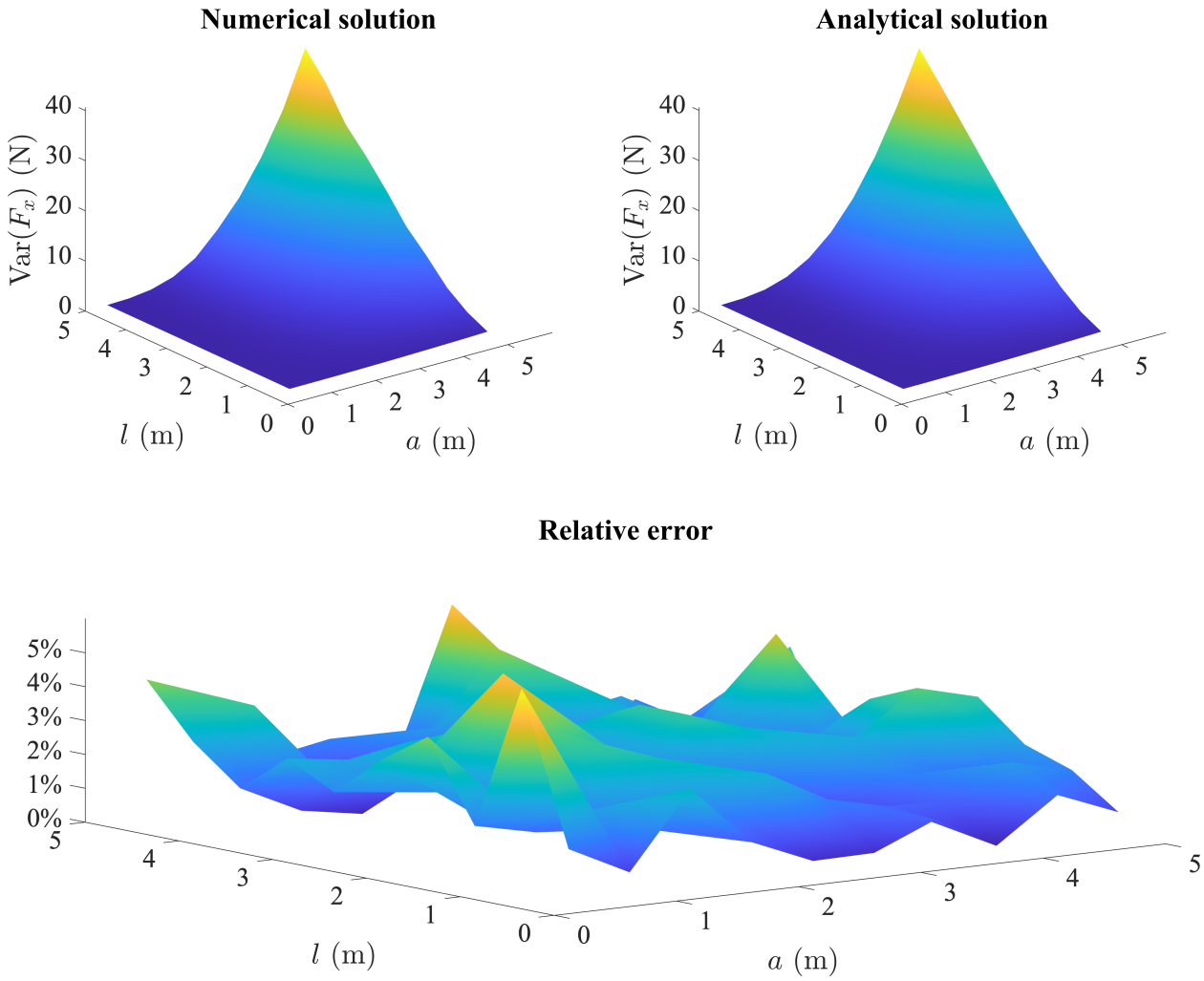

Fig. 4. Variance of the friction force in pure translation case.

Note that because of $\mu_T = 0$ as computed in Eq.8, the variable of the same dimension $|\mu_F| a_m$ is used instead at the denominator in Eq.15, where $a_m = a/\sqrt{2}$ is the mean square distance concerning the centre of the contact interface. We note that such modifications to the definition of CV will deviate from its original mathematical definition. However, the name "$\mathrm{CV_T}$" is still adopted for consistency, so as the use of $\mathrm{CV}_{\|\hat{\mathbf{F}}\|}$ in the pure rotation case in Eq.26. The explicit form of Eq.14 and Eq.15 can be derived directly, as functions of the ratio $l\,/\,a$, from Eq.6∼9. By setting $t = l\,/\,a$ these variables can be expressed as

$$\begin{aligned}\mathrm{CV}_{\|\mathbf{F}\|}(t) = \frac{\sigma_{\mathbb{H}}}{4\,\mu_{\mathbb{H}}}\Big\{&4\pi\mathrm{erf}^2(\frac{2}{t})\,t^2 + 4\sqrt{\pi}\mathrm{erf}(\frac{2}{t})(\mathrm{e}^{-\frac{4}{t^2}} - 1)t^3 \\ &+ (1 - 2\mathrm{e}^{-\frac{4}{t^2}} + \mathrm{e}^{-\frac{8}{t^2}})t^4\Big\}^{\frac{1}{2}}\end{aligned} \tag{16}$$

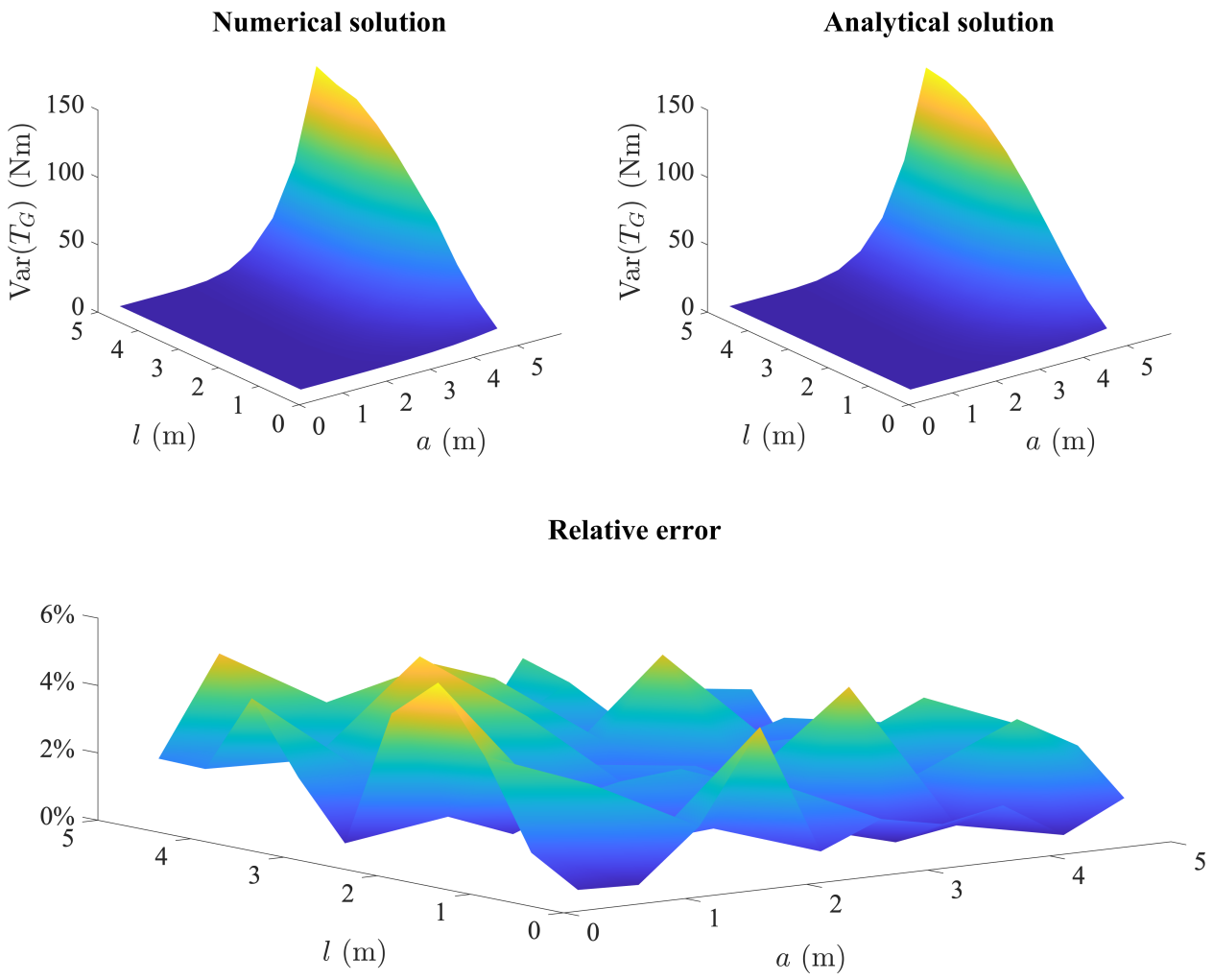

Fig. 5. Variance of the torque in pure translation case.

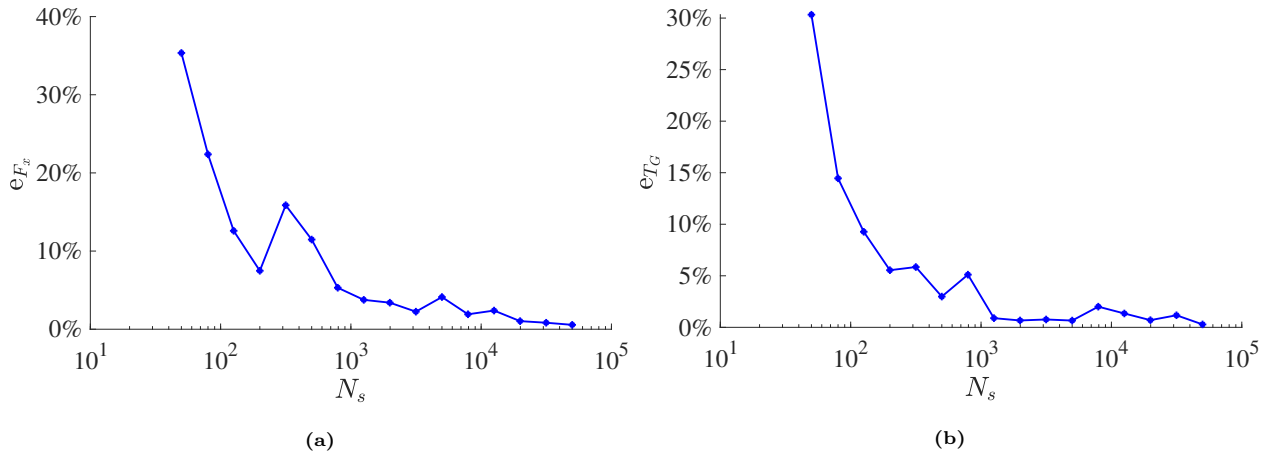

Fig. 6. (a) e_{F_x} and (b) e_{T_G} with sample size N

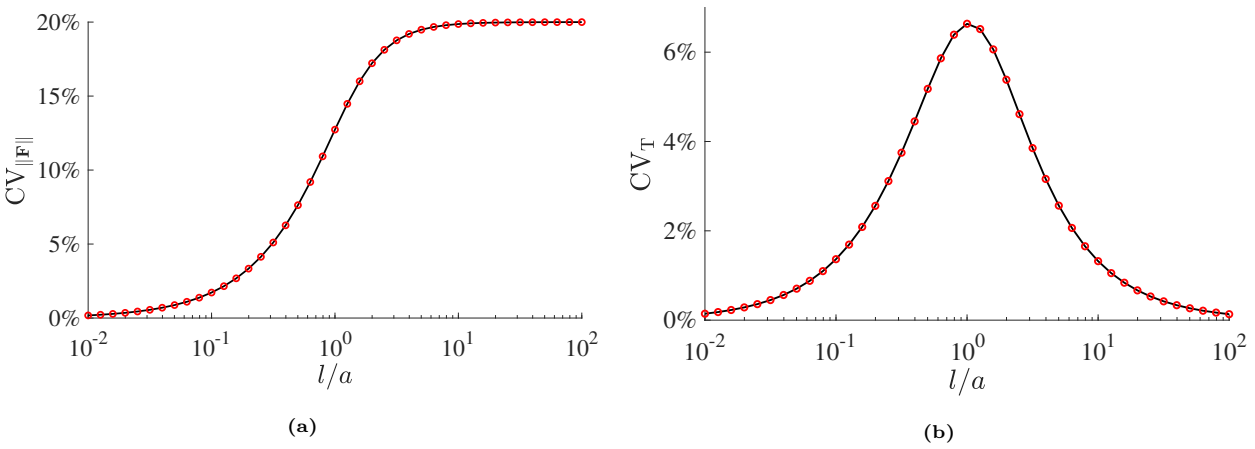

Fig. 7. CVs of the friction force and torque in pure translation. (a) $\mathrm{CV}_{\|\mathbf{F}\|}$; (b) CV_{T}.

$$\begin{aligned}\mathrm{CV}_{\mathrm{T}}(t) = \frac{\sqrt{2}\,\sigma_{\mathbb{H}}}{4\,\mu_{\mathbb{H}}}\Big\{&\frac{4\pi}{3}\mathrm{erf}^2(\frac{2}{t})\,t^2 + \frac{4\sqrt{\pi}}{3}\mathrm{erf}(\frac{2}{t})(\mathrm{e}^{-\frac{4}{t^2}} - 2)t^3 \\ &+ (1 - \frac{4}{3}\mathrm{e}^{-\frac{4}{t^2}} + \frac{1}{3}\mathrm{e}^{-\frac{8}{t^2}})t^4 + \frac{\sqrt{\pi}}{3}\mathrm{erf}(\frac{2}{t})(1 - \mathrm{e}^{-\frac{4}{t^2}})t^5 \\ &+ (\frac{1}{3}\mathrm{e}^{-\frac{4}{t^2}} - \frac{1}{6}\mathrm{e}^{-\frac{8}{t^2}} - \frac{1}{6})t^6\Big\}^{\frac{1}{2}},\end{aligned} \tag{17}$$

making use of the limits and derivative of Gauss error function as

$$\begin{aligned}\lim_{x\to+\infty}\mathrm{erf}(x) &= 1 \\ \lim_{x\to 0}\mathrm{erf}(x) &= 0 \\ \frac{\mathrm{d}\,\mathrm{erf}(x)}{\mathrm{d}x} &= \frac{2}{\sqrt{\pi}}\mathrm{e}^{-x^2},\end{aligned} \tag{18}$$

the limits of $\mathrm{CV}_{\|\mathbf{F}\|}$ and CV_{T} can be obtained as

$$\begin{aligned}\lim_{t\to 0}\mathrm{CV}_{\|\mathbf{F}\|}(t) &= 0 \\ \lim_{t\to+\infty}\mathrm{CV}_{\|\mathbf{F}\|}(t) &= \frac{\sigma_{\mathbb{H}}}{\mu_{\mathbb{H}}} \\ \lim_{t\to 0}\mathrm{CV}_{\mathrm{T}}(t) &= 0 \\ \lim_{t\to+\infty}\mathrm{CV}_{\mathrm{T}}(t) &= 0.\end{aligned} \tag{19}$$

Hence, the results can be collected into more concise dimensionless figures, as shown in Fig.7. As Fig.7a illustrates, $\mathrm{CV}_{\|\mathbf{F}\|}$ is a monotonic function of the ratio l/a starting from a small value but increasing rapidly as l/a takes increasing values from 0.3 to 10. This result means that when the ratio l/a is of a low value, say lower than 0.3, the friction force will not deviate from its mean value by 5%. Consequently, the randomness in COF will not have much influence on the macroscopic friction force. Thus we can set 0.3 as a reasonable threshold to determine whether it is worthy of taking the randomness of COF into account. On the other hand, when l/a is of a high value such as $l/a > 10$, the deviation of the friction force from its mean value

levels off at around 20%, which corresponds to the CV used to generate the COF random field as its infinite limits shown in Eq.19(2). The reason for this levelling off is that when the correlation length of the random field is much larger than the characteristic length of the same field, the variables in the random field will tend to become spatially uniform (but still random) over the interface because in that circumstance each variable is highly correlated with their adjacent counterparts. It can also be observed that $\mathrm{CV}_{\|\mathbf{F}\|}$ tends to zero as l/a tends to zero. Indeed for a very small correlation length, a spatial homogenisation takes place and the global random force tends to a deterministic one (equal to its mean value). The coefficient of variation of the torque exhibited in Fig.7b, however, shows a different trend from that of the friction force. $\mathrm{CV_T}$ increases first but drops down with the increase of the ratio l/a and it reaches its maximum value when l and a have close values. As the ratio l/a becomes large the deviation tends to be 0. It makes sense because as the COF random field tends to be spatially uniform, no resultant torque will be generated. Furthermore, as the maximum of $\mathrm{CV_T}$ is lower than 5%, it becomes a problem-depend task to determine the importance of the torque. For example, if the problem to be solved is position-sensitive or energy-sensitive, it would be necessary to take the torque into account because it would lead to rotation and energy dissipation. Otherwise, its influence may be negligible. As for the force, it can be observed that $\mathrm{CV_T}$ tends to zero as l/a tends to zero for the same reasons.

In summary, when $l/a < 0.3$ the randomness in COF has little impact on the friction force and torque, and deterministic friction laws are still usable. When $0.3 < l/a < 10$ we should consider taking this randomness into account and model it as a random field as it causes apparent deviations from deterministic solutions. When $l > 10$ this randomness is non-negligible whereas it may behave more like a random variable than a random field (because the random field tends to be spatially uniform).

2.2. Pure rotation

2.2.1. Theoretical formulation

In pure rotation case, the plate has a constant angular velocity $\boldsymbol{\omega} = \omega\ \mathbf{e_z}$ as shown in Fig.2b. The generated friction force and torque at the centre of mass can then be derived as:

$$\hat{\mathbf{F}}_{\mathbf{G}} = -\iint_S P\mathbb{H}(\mathbf{x})\frac{\boldsymbol{\omega}\times\mathbf{x}}{|\boldsymbol{\omega}\times\mathbf{x}|}\mathrm{d}S = -\iint_S P\mathbb{H}(\mathbf{x})\frac{\mathbf{x}}{|\mathbf{x}|}\mathrm{d}S \tag{20}$$

$$\hat{\mathbf{T}}_{\mathbf{G}} = -\iint_S P\mathbb{H}(\mathbf{x})\frac{\mathbf{x}\times(\boldsymbol{\omega}\times\mathbf{x})}{|\boldsymbol{\omega}\times\mathbf{x}|}\mathrm{d}S = -\iint_S P\mathbb{H}(\mathbf{x})|\mathbf{x}|\mathrm{d}S\ \mathbf{e_z}\ , \tag{21}$$

The friction force contains two components, namely $\hat{\mathbf{F}}_{\mathbf{G}} = \hat{F}_x\,\mathbf{e_x} + \hat{F}_y\,\mathbf{e_y}$ and their first moment can be obtained through Eq.20 as $\mathbb{E}[\hat{F}_x] = \mathbb{E}[\hat{F}_y] = 0$. The torque is $\hat{\mathbf{T}}_{\mathbf{G}} = \hat{T}_G\mathbf{e_z}$ with its first moment being

$$\mathbb{E}[\hat{T}_G] = -\iint_S P\mu_{\mathbb{H}}|\mathbf{x}|\mathrm{d}S. \tag{22}$$

The second moment of the friction forces and torque can be derived as

$$\mathbb{V}ar[\hat{F}_x] = \sigma^2_{\hat{F}_x} = \iint_{S'}\iint_S P^2\mathrm{C}_{\mathbb{H}}(\mathbf{x},\mathbf{x}')\,\frac{x}{|\mathbf{x}|}\,\frac{x'}{|\mathbf{x}'|}\,\mathrm{d}S\mathrm{d}S' \tag{23}$$

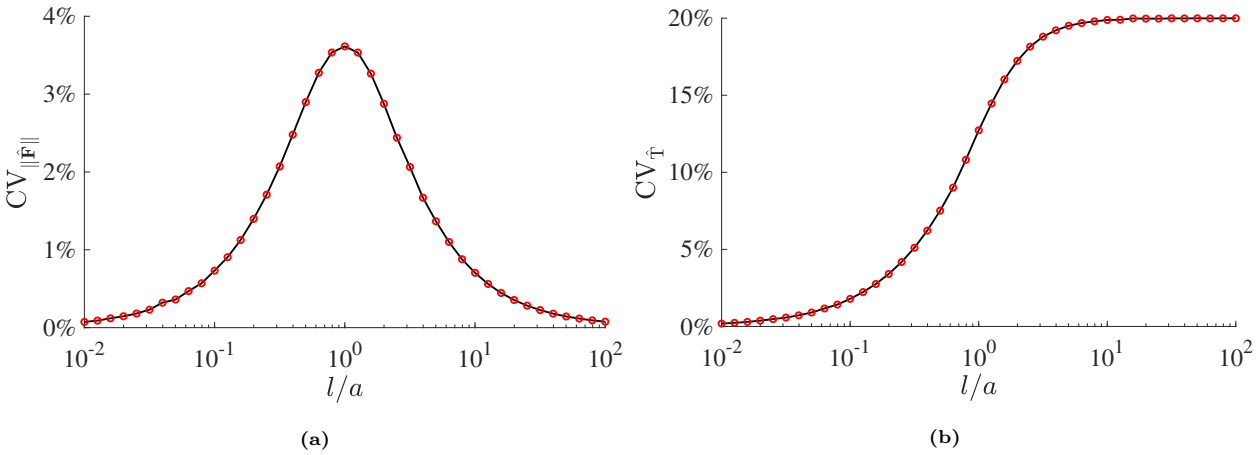

Fig. 8. CV of the friction force and torque with l/a in pure rotation case. (a) $\mathrm{CV}_{\|\hat{\mathbf{F}}\|}$; (b) $\mathrm{CV}_{\hat{\mathrm{T}}}$.

$$\mathbb{V}ar[\hat{F}_y] = \sigma^2_{\hat{F}_y} = \iint_{S'} \iint_{S} P^2 \mathrm{C}_{\mathbb{H}}(\mathbf{x}, \mathbf{x}') \frac{y}{|\mathbf{y}|} \frac{y'}{|\mathbf{y}'|} \mathrm{d}S\mathrm{d}S' \tag{24}$$

$$\mathbb{V}ar[\hat{T}_G] = \sigma^2_{\hat{T}} = \iint_{S'} \iint_{S} P^2 \mathrm{C}_{\mathbb{H}}(\mathbf{x}, \mathbf{x}') |\mathbf{x}||\mathbf{x}'| \mathrm{d}S\mathrm{d}S'. \tag{25}$$

However, unlike in the pure translation case, Eq.22 $\sim$ Eq.25 can not be evaluated analytically. As a consequence, investigations about their statistical properties will be carried out based on numerical simulations.

2.2.2. CVs *of friction force and torque in pure rotation case*

The CVs of the friction forces and torque are defined in Eq.26 and Eq.27. For the same reason as in Sec.2.1.4, the denominator of force CVs are replaced with $|\mu_{\hat{T}}|$ and an a_m is multiplied in its numerator to form a dimensionless variable. We note that although explicit formulations are not available, the dependence of $\mathrm{CV}_{\|\hat{\mathbf{F}}\|}$ and $\mathrm{CV}_{\hat{\mathrm{T}}}$ on the ratio l/a can be deduced straightforwardly as we take $\mathbf{w} = \mathbf{x}/l$ and $\mathbf{w}' = \mathbf{x}'/l$ into Eq.22 $\sim$ Eq.25 and nondimensionalise the body dimensions with the correlation length.

$$\mathrm{CV}_{\|\hat{\mathbf{F}}\|} = \frac{\sigma_{\|\hat{\mathbf{F}}\|}\, a_m}{|\mu_{\hat{T}}|} \tag{26}$$

$$\mathrm{CV}_{\hat{\mathrm{T}}} = \frac{\sigma_{\hat{T}}}{|\mu_{\hat{T}}|}. \tag{27}$$

The results are collected into Fig.8. The results show a familiar trend as in the pure translation case. However, the role of the friction force and torque have interchanged, showing a duality between the pure translation case and the pure rotation case. This duality is shown directly in Fig.9. Note that the different maximum values of CV_{T} and $\mathrm{CV}_{\|\hat{\mathbf{F}}\|}$ may come from the scaling methods used in constructing those dimensionless variables. Therefore, the conclusions and interpretations that have been drawn in Sec.2.1.4 for the pure translation case can immediately be applied for this pure rotational case.

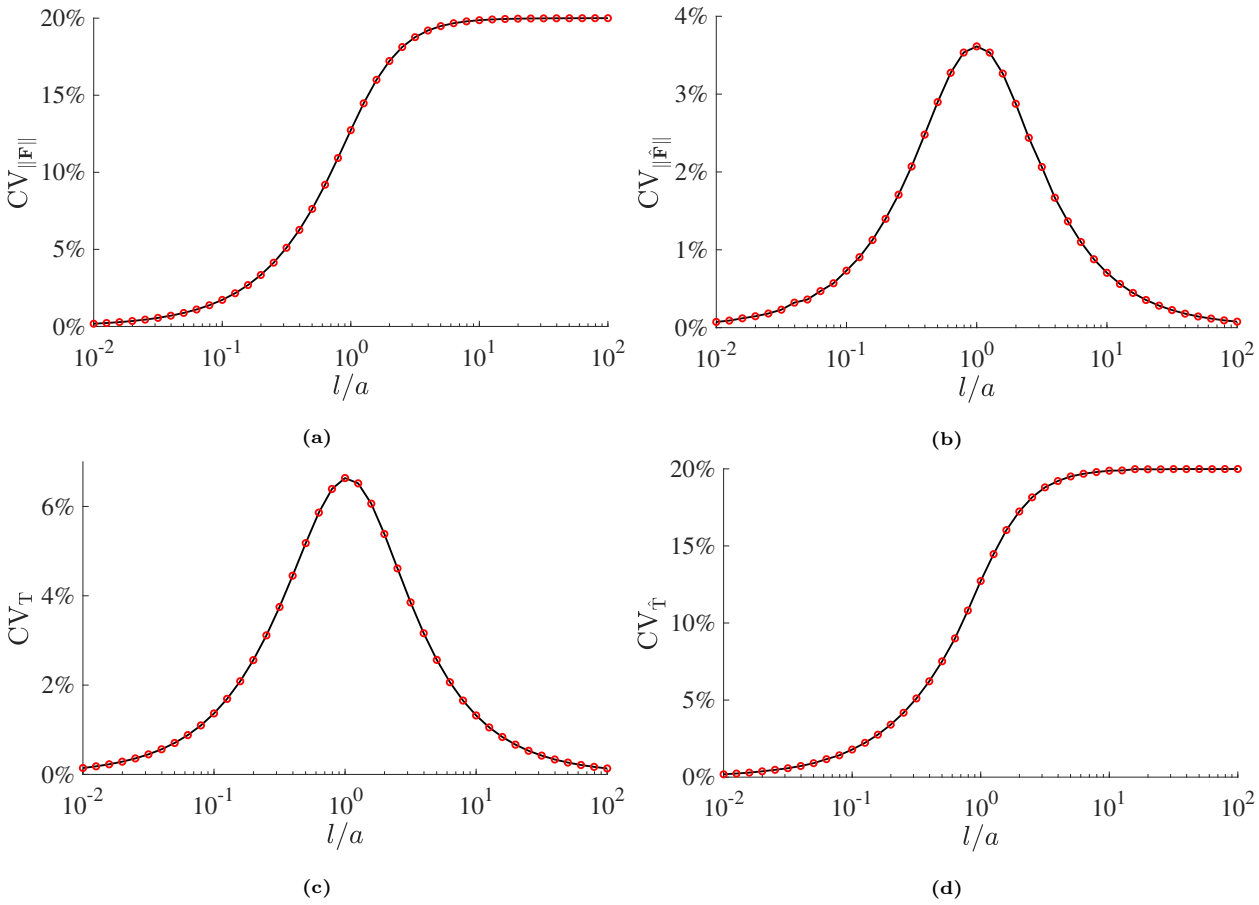

Fig. 9. Duality of CVs between pure translation and pure rotation. (a) $\mathrm{CV}_{\|\mathbf{F}\|}$ with l/a; (b) $\mathrm{CV}_{\|\hat{\mathbf{F}}\|}$ with l/a; (c) CV_{T} with l/a; (d) $\mathrm{CV}_{\hat{\mathrm{T}}}$ with l/a.

2.3. General planar motion

2.3.1. Theoretical formulation

In the third case, we apply a general planar motion, namely a combination of translation and rotation, to the plate, with the translating and rotating velocity $\tilde{\mathbf{v}}$ and $\tilde{\boldsymbol{\omega}}$ correspondingly shown in Fig.2c. The translating velocity is again assumed to be parallel to $\mathbf{e_x}$ in the body-fixed frame, e.g. $\tilde{\mathbf{v}} = \tilde{v}\mathbf{e_x}$, and the rotating velocity to $\mathbf{e_z}$, e.g. $\tilde{\boldsymbol{\omega}} = \tilde{\omega}\mathbf{e_z}$. Without loss of generality, we set $\tilde{v} = \rho^\star\tilde{\omega}$, where $\rho^\star \in \mathbb{R}$ is an arbitrary coefficient with the unit of length. The resultant random friction force and torque can thus be expressed as

$$\begin{aligned}\tilde{\mathbf{F}}_{\mathbf{G}} &= -\iint_S P\mathbb{H}(\mathbf{x})\frac{\tilde{\boldsymbol{\omega}}\times\mathbf{x}+\tilde{\mathbf{v}}}{|\tilde{\boldsymbol{\omega}}\times\mathbf{x}+\tilde{\mathbf{v}}|}\mathrm{d}S \\ &= \iint_S P\mathbb{H}(\mathbf{x})\frac{-(\rho^\star-y)}{\sqrt{(\rho^\star-y)^2+x^2}}\mathrm{d}S\mathbf{e_x} + \iint_S P\mathbb{H}(\mathbf{x})\frac{-x}{\sqrt{(\rho^\star-y)^2+x^2}}\mathrm{d}S\mathbf{e_y}\end{aligned} \tag{28}$$

$$\tilde{\mathbf{T}}_{\mathbf{G}} = -\iint_S P\mathbb{H}(\mathbf{x})\frac{\mathbf{x}\times(\tilde{\boldsymbol{\omega}}\times\mathbf{x}+\tilde{\mathbf{v}})}{|\tilde{\boldsymbol{\omega}}\times\mathbf{x}+\tilde{\mathbf{v}}|}\mathrm{d}S = \iint_S P\mathbb{H}(\mathbf{x})\frac{-(x^2-\rho^\star y+y^2)}{\sqrt{(\rho^\star-y)^2+x^2}}\mathrm{d}S\mathbf{e_z}. \tag{29}$$

As seen in Eq.28 and Eq.29, the frictional force and torque have dependencies on $\rho^\star$ or on the velocity state of the plate, which is essentially different from pure translation and pure rotation cases. Therefore, the role that $\rho^\star$ plays in the results is going to be examined in the following analysis. The closed-form formulations for the statistical properties of friction force and torque are by no means available like in the pure rotation case, thus they will be studied by numerical approach.

2.3.2. CVs *of friction force and torque in general planar motion case*

The CVs of the friction force and torque in general planar motion case are defined by the original definitions, as shown in Eq.30. These definitions make sense as long as $\rho^\star$ is neither too large nor too small, which would make the mean value of one of the variables (friction force or torque) approach to zero and the general planar motion case drop to pure translation or pure rotation case.

$$\mathrm{CV}_{\|\tilde{\mathbf{F}}\|} = \frac{\sigma_{\|\tilde{\mathbf{F}}\|}}{\mu_{\|\tilde{\mathbf{F}}\|}},\ \mathrm{CV}_{\tilde{\mathrm{T}}} = \frac{\sigma_{\tilde{T}}}{\mu_{\tilde{T}}}\ , \tag{30}$$

Similar to the derivations in the pure rotation case, the CVs are functions of the ratio l/a can be simply justified by dimensional analysis and are omitted here. The resultant $\mathrm{CV}_{\|\tilde{\mathbf{F}}\|}$ and $\mathrm{CV}_{\tilde{\mathrm{T}}}$ with l/a are shown in Fig.10 concerning ratio $\rho^\star/a$ ranging from 0.1 to 5.0. The results interestingly show a combined effect of

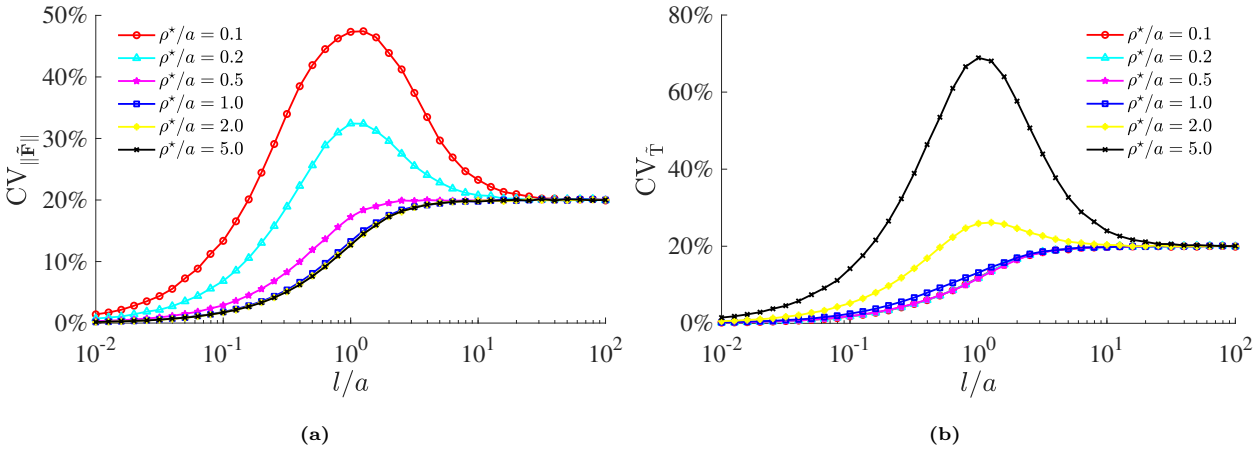

Fig. 10. (a) $\mathrm{CV}_{\|\tilde{\mathbf{F}}\|}$ and (b) $\mathrm{CV}_{\tilde{\mathrm{T}}}$

the results of the previous cases (pure translation and pure rotation) already have been investigated. For $\mathrm{CV}_{\|\tilde{\mathbf{F}}\|}$, the trend of its value is "rotation-dominated" when $\rho^\star/a$ is below 0.5, as it shows a similarity with the pure rotation case that the curve increases first and reaches the extremity at around $l/a = 1$ and then decreases, except for the fact that it finally converges to 20% when l/a becomes large while in the pure rotation case the limit being zero. Moreover, the peak value goes larger as $\rho^\star/a$ decreases and can be as large as near 50%, showing the friction force being heavily fluctuated caused by the small translating velocity component compared to rotating velocity component. On the opposite, the trend is "translation-dominated" when $\rho^\star/a$ is above 0.5 as its value increases monotonically with l/a and finally stabilises at 20%. For $\mathrm{CV}_{\tilde{\mathrm{T}}}$, the overall effect of $\rho^\star/a$ is the same as $\mathrm{CV}_{\|\tilde{\mathbf{F}}\|}$ but the threshold to determine a dominating motion for the

CV of torque is more likely to be $\rho^\star/a = 2.0$ rather than 0.5 for that of friction force, as the trend becomes "rotation-dominated" when $\rho^\star/a < 2.0$, and "translation-dominated" otherwise. The extremity, if exists, shows again at around $l/a = 1$ and the peak value increases with $\rho^\star/a$ as the fluctuation in the torque is more severe when the rotating velocity becomes too small compared against the translating velocity. However, the converged value is the same (20%) when l/a tends to be large. The reason for this convergence is that when the translating motion and rotating motion are comparable, in other words, when neither motion of the two directions is negligible, and when the correlation length of the COF field is much larger than the characteristic length of the body, the resultant friction force and torque are linearly dependent on the COF (which is more of a random variable rather than random field in this case) and then show the same statistical property with the COF (like Eq.19.2 in the limit analysis).

The question of when to model COF as a random field in the general planar motion case can not be answered in a general way because the results vary with the ratio $\rho^\star/a$. When $0.5 \leq \rho^\star/a \leq 2$, the thresholds we set in previous sections are still applicable, which is to model the COF as a deterministic variable when $l/a < 0.3$, as a random field when $0.3 \leq l/a \leq 10$ and as a random variable when $l/a \geq 10$. However, if $\rho^\star/a$ goes beyond the range $[0.5, 2]$, the threshold should be determined carefully based on the specific problem, as the variation can be significant even with a small l/a value. Therefore, in those cases, the lower threshold is likely to decrease, but the higher threshold could remain unchanged, as when l/a approaches 10, both the CVs of friction force and torque come to converge.

2.3.3. Investigation on the form of the correlation function

Till now, our findings are mainly based on the Gaussian type correlation function as represented by Eq.1. In this section, we are going to discuss the impact of the form of the correlation function on our results and to see if our conclusions rely on a specific form of the correlation function.

A general correlation function has the form of

$$\tilde{\mathrm{R}}_{\mathbb{H}}(\mathbf{x}, \mathbf{x}') = \mathrm{e}^{-\left(\frac{\|\mathbf{x}-\mathbf{x}'\|}{l}\right)^n}, \tag{31}$$

where n is the exponent index as we set $n = 2$ in all the above investigations. Herein we set $n \in \{1, 2, 3, 4\}$ to see if changing the exponent index could yield a different result. For generality, we choose two translating and rotating velocity pairs as $\rho^\star/a \in \{0.1, 1.0\}$ and the resultant $\mathrm{CV}_{\|\tilde{\mathbf{F}}\|}$ and $\mathrm{CV}_{\tilde{\mathrm{T}}}$ are compared concerning different n, as depicted in Fig.11. For $\rho^\star/a = 0.1$, it can be seen that as n increases the peak value of $\mathrm{CV}_{\|\tilde{\mathbf{F}}\|}$ increases and the bandwidth decreases gradually and $\mathrm{CV}_{\tilde{\mathrm{T}}}$ converges to its limit faster. For $\rho^\star/a = 1.0$, both the $\mathrm{CV}_{\|\tilde{\mathbf{F}}\|}$ and $\mathrm{CV}_{\tilde{\mathrm{T}}}$ converge faster when n increases, while the general trend stays the same. These results demonstrate that the form of the correlation function will affect only local properties of CVs of friction force and torque (peak values, bandwidth and convergence rate) but not the general trend. So the analysis on the Gaussian type correlation function may be readily transferred on other forms of the correlation function, although the specific thresholds may change and need to be calibrated according to the velocity pairs under investigation.

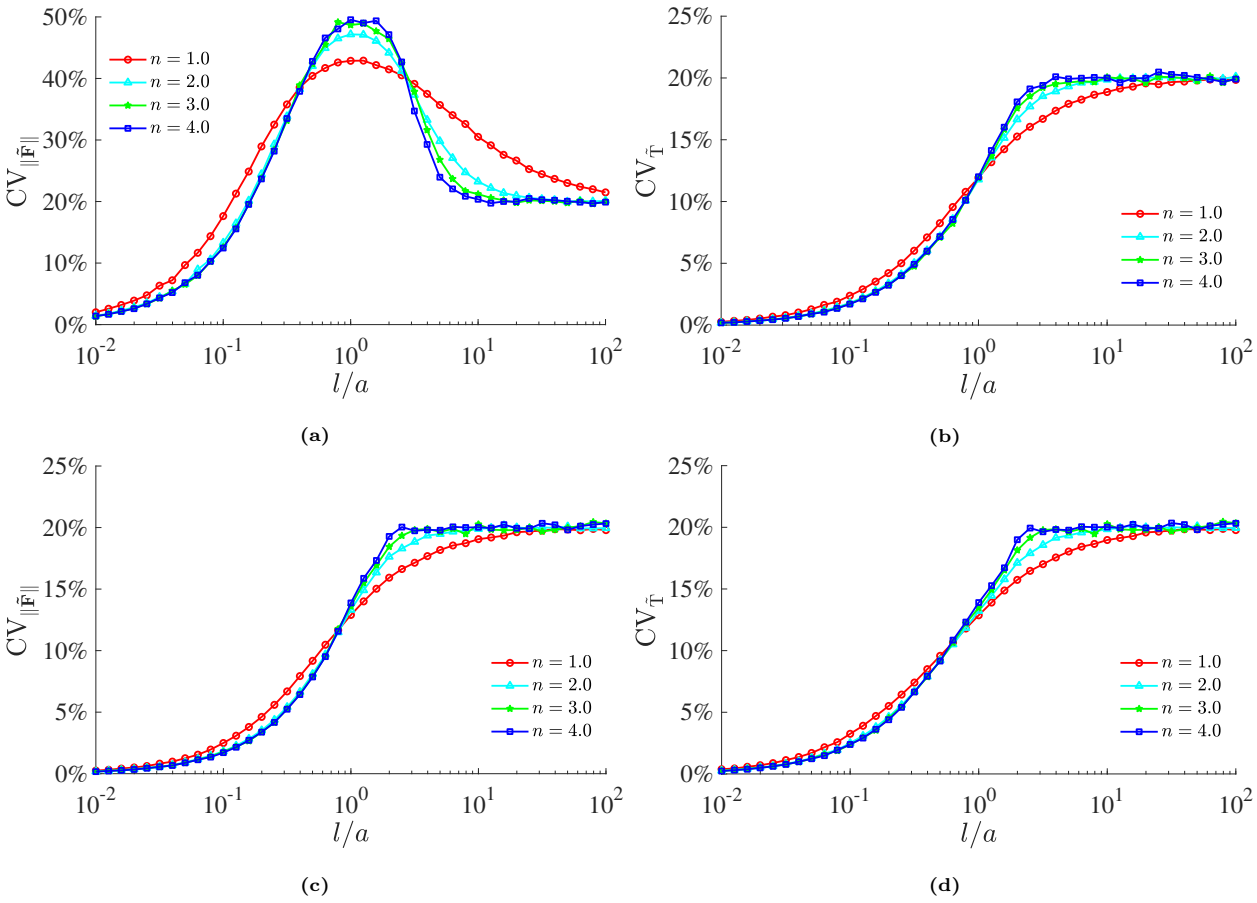

Fig. 11. (a),(b)$\mathrm{CV}_{\|\tilde{\mathbf{F}}\|}$ and $\mathrm{CV}_{\tilde{\mathrm{T}}}$ with respect to n for $\rho^{\star}/a = 0.1$; (c),(d)$\mathrm{CV}_{\|\tilde{\mathbf{F}}\|}$ and $\mathrm{CV}_{\tilde{\mathrm{T}}}$ with respect to n for $\rho^{\star}/a = 1.0$.

3. Application: a crank-slider model

An application on a crank-slider model is investigated to further illustrate the impact of the random field modelling of COF on energy dissipation during the motion. The crank-slider model is shown in Fig.12. The motion of the slider is constrained by the track. The bottom and side surfaces of the slider are considered as rough surfaces, whereas the surface of the track is assumed to be rigid flat. In such assumptions, the COF of the interface between the slider and the track will locally depend on the slider. A random field with correlation function as in Eq.1 is used to represent the COF of the interface. During the motion of the slider, as discussed in Sec.2.1, the slider endures a torque, which would bring it in contact with side walls at two points of the track as shown in Fig.13. The torque and the normal force at side wall thus satisfy the relation in Eq.32, where a is half of the length of the bottom surface of the slider and F_{NS} is the normal contact force as represented in Fig.13.

$$T = 2aF_{NS}. \tag{32}$$

The differential equation of the system is formulated by using Lagrange equations of second kind with geometric constrains. Details of derivation of the equation can be found in Appendix B. By setting angles

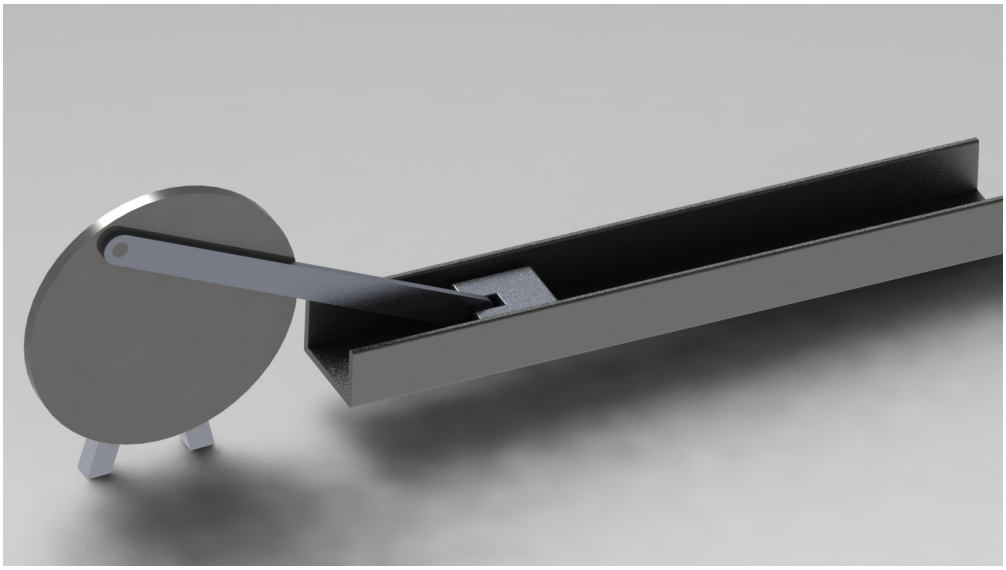

(a)

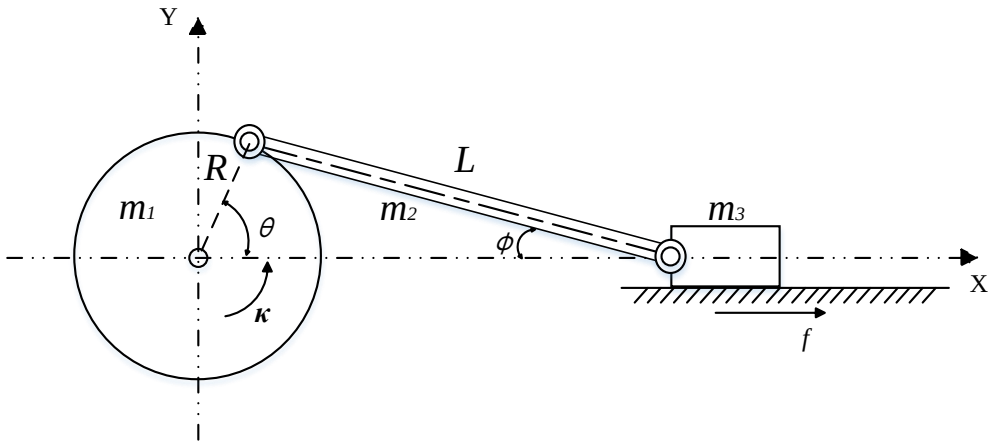

(b)

Fig. 12. Crank slider model (a) 3D form; (b)2D form.

θ and ϕ as generalized coordinates, namely $\mathbf{q} = [\theta, \phi]^T$, the differential equation can be expressed in matrix form as

$$\mathbf{M}(\mathbf{q})\ddot{\mathbf{q}} + \mathbf{F}(\mathbf{q}, \dot{\mathbf{q}}) + \mathbf{Q}_C = \mathbf{Q}_A \ , \tag{33}$$

where $\mathbf{M}(\mathbf{q})$ is the mass matrix, $\mathbf{F}(\mathbf{q}, \dot{\mathbf{q}})$ is the force vector, $\mathbf{Q}_C$ is the generalized constraint reaction force and $\mathbf{Q}_A$ is the generalized force. Details of the above variables are given in Appendix B. After calculating the dynamical response of the system, the displacement of the slider is obtained as

$$x_3 = R\cos(\theta) + L\cos(\phi) \ , \tag{34}$$

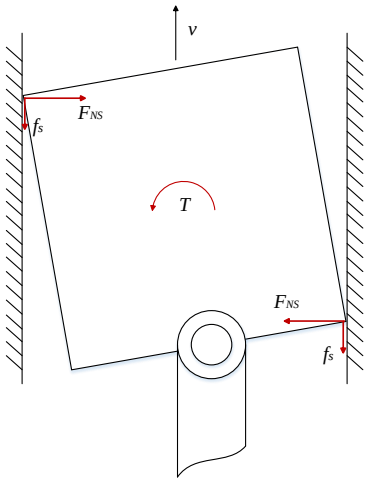

Fig. 13. Friction at side walls.

and the energy dissipations caused by frictions can be expressed as

$$\begin{aligned} E_s &= \int_0^t |f_s \cdot \dot{x_3}| \mathrm{d}t \\ E_b &= \int_0^t |f_b \cdot \dot{x_3}| \mathrm{d}t \ , \end{aligned} \tag{35}$$

where f_s and f_b are the friction forces at the side and bottom of the slider, respectively, and E_s and E_b are the corresponding energy dissipations. The COF of the contact interface between the slider and the track is constructed using random field discretization technique described in Sec.2.1.3. The parameters used in the simulations are given in Table 1. The initial conditions are set as $\mathbf{q_0} = [\theta_0, \phi_0]^T = [-1.0472, -0.5464]^T$ and $\dot{\mathbf{q}}_\mathbf{0} = [\dot{\theta}_0, \dot{\phi}_0] = [10.000, 3.5172]$. The simulation time is $t = 2s$. The ratio of the correlation length to the characteristic length, l/a, is taken values from$[10^{-1}, 10^2]$, and at each value of l/a 50 realizations are computed to obtain estimated energy dissipation.

Table 1: Parameters in crank-slide model

Parameter	Value	Parameter	Value	Parameter	Value
m_1 (kg)	0.3	m_2 (kg)	0.3	m_3 (kg)	0.3
R (m)	0.3	L (m)	0.5	a (m)	0.3
κ (Nm)	0.5	$\mu_{\mathbb{H}}$	0.5	$\sigma^2_{\mathbb{H}}$	0.01

Fig.14 and Fig.15 illustrate the mean value and standard deviation (Std) of the energy dissipations from the friction of the bottom and side of the contact interfaces with respect to different ratio l/a. The results are compared with those of the deterministic model, in which the COF is set as a constant value equal to the mean value of the COF in the random model. Several observations can be made from Fig.14. First of all, the mean value of E_b from the random model is very close to the deterministic result when $l/a < 0.3$, in the mean time the standard deviation is of a relatively low value. Second, as the ratio l/a becomes larger,

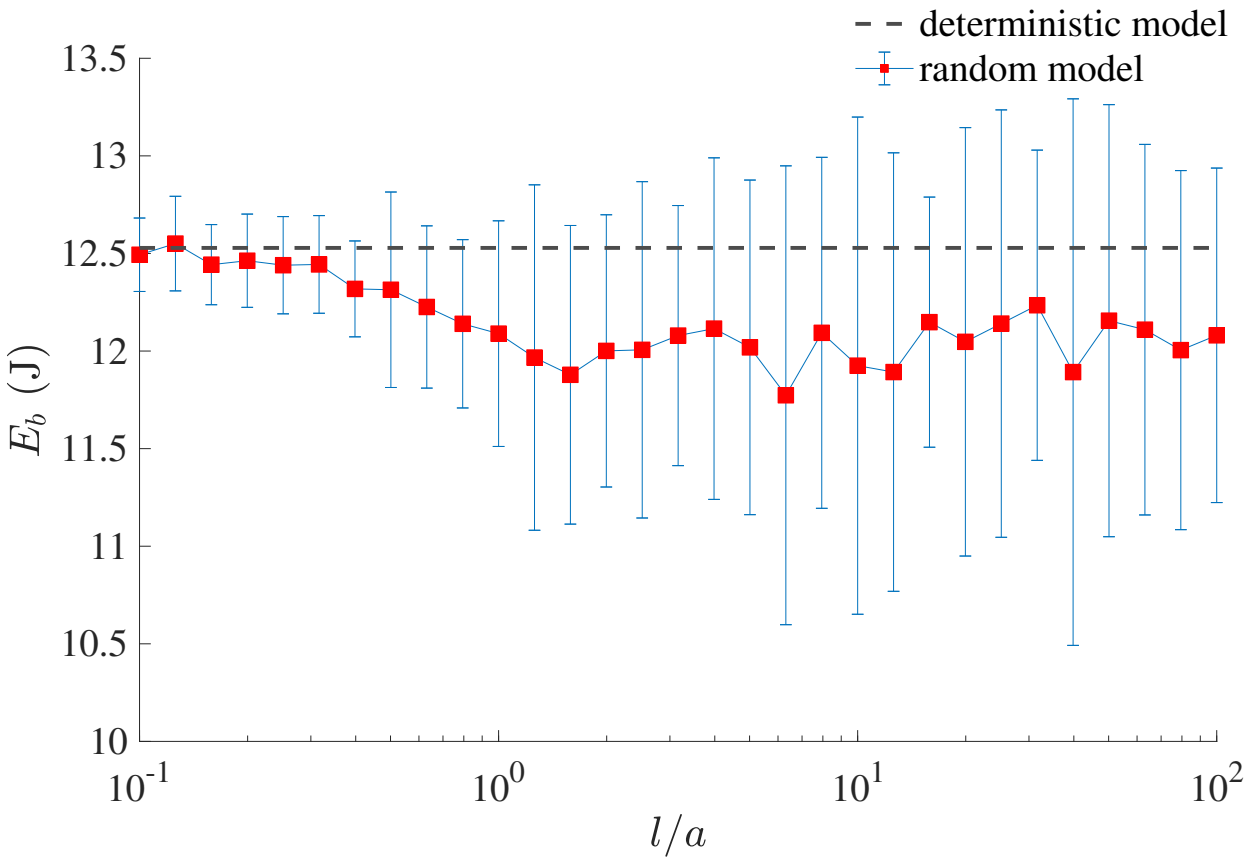

Fig. 14. Energy dissipation of bottom friction. Deterministic model (dashed line) and random model (mean value in squared line +/- the standard deviation in error bars).

the mean value of E_b from the random model shows apparent deviation from the deterministic result, and its standard deviation also increases significantly. Finally, when l/a increases approximately over twice the mean value and standard deviation of the energy dissipation stabilizes. Since this energy is generated by bottom friction force (and not the torque), these results are consistent with our previous theoretical analysis.

In Fig.15, the energy dissipation caused by side friction E_s, which comes from the torque generated through motion, exhibits a different trend with l/a compared with its counterpart E_b. As l/a grows from 10^{-1} to 1, both its mean and standard deviation increase and reach a maximum value when l/a is nearly 1. However, as l/a continuously increases they both shrink and finally approach 0 when l/a is as large as 10^2. These results again are in agreement with our analysis about CV of torque in the pure translation case. Moreover, E_s may take a percentage up to 5% of the total energy dissipation from all the scenarios, so this dissipation should be taken seriously into account in an energy-sensitive system.

4. Conclusions

In this paper, the inherent random fluctuation of the friction coefficient in dry-frictional phenomena is modelled by a random field, and the impact of the correlation length l of the random field and the

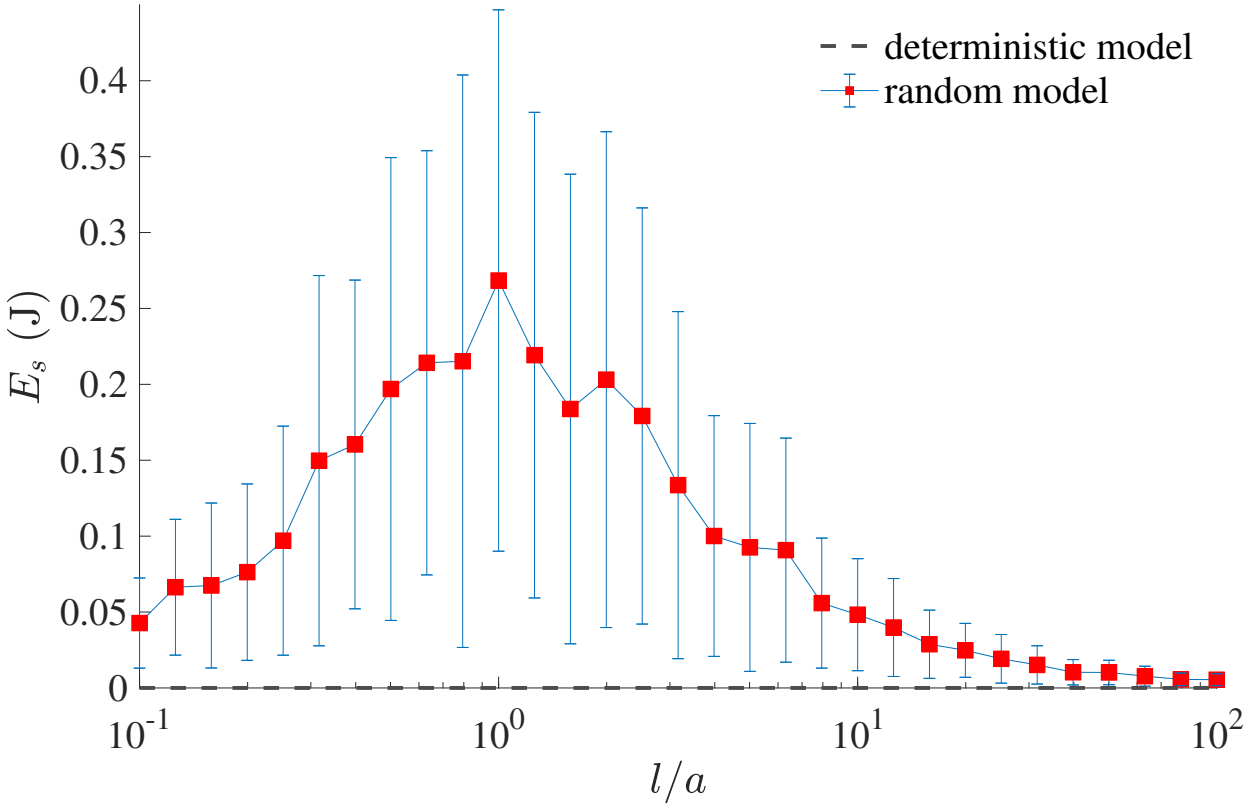

Fig. 15. Energy dissipation of side friction. Deterministic model (black dashed line) and random model (mean value in red squared +/- the standard deviation in blue lines).

characteristic length a of the contact interface on the statistical properties of the global friction force and torque is investigated. Theoretical analysis and numerical simulations are conducted in three different planar sliding problem settings: the pure translation, pure rotation motion and the general planar motion of the plate. It has been shown that when the correlation length is much smaller than the characteristic length of the interface then a spatial homogenisation takes place and the randomness of the coefficient of variation can be neglected and replaced by a deterministic one. When the correlation length is much larger than the characteristic length of the interface, the spatial fluctuations can be neglected and the coefficient of friction random field can be replaced by a random variable (instead of a random field). Finally when the correlation is of the same order of magnitude than the characteristic length, then the spatial fluctuations of the coefficient of friction is not negligible and has be modelled using a random field.

An application on a crank-slider system is used to illustrate these findings from the energy dissipation perspective. It is found that, as expected from the theoretical analysis, when the ratio satisfies $l/a < 0.3$, the resulting energy dissipation from a random model is comparable to that from a deterministic model, while possessing a low standard deviation. When $l/a > 0.3$ the results of random models become distinctive and the standard deviation of dissipated energy caused by the torque (or friction force) can not be neglected. Finally, when $l/a > 10$ the friction coefficient tends to be spatially uniform because of strong correlation

among the whole interface and can be replaced by a random variable instead of a random field.

Acknowledgment

The first author H. Hu gratefully acknowledges the financial support from the University of Liverpool and China Scholarship Council Awards (CSC NO.201906230311).

Appendix A Approximate construction of the probability distribution of the random variables F_x and T_G

In a discrete perspective, the random friction force (of its x-component) and the random torque can be represented as

$$F_x = -\lim_{n\to+\infty}\sum_{i=1}^{n} P\,\mathbb{H}(\mathbf{x}_i)\,\mathrm{d}S_i \tag{A.1}$$

$$T_G = -\lim_{n\to+\infty}\sum_{i=1}^{n} P\,\mathbb{H}(\mathbf{x}_i)\cdot y_i\,\mathrm{d}S_i. \tag{A.2}$$

Since the COF random field, $\mathbb{H}(\mathbf{x})$, has a lognormal probability distribution, F_x can be seen as a summation of correlated lognormal random variables, with a negative sign. It has been shown in the literature that the summation of correlated lognormal random variables with positive coefficients converge in probability to a single lognormal random distribution [37]. In general, for a random variable $S=\sum_{i=1}^{n} c_i\,\tau_i$, where τ_i is a lognormal random variable with mean value μ_{τ_i} and variance $\sigma^2_{\tau_i}$, and c_i the positive coefficient and the correlation function among τ_i satisfying $Cov(\tau_i,\tau_j)=\sigma_{(\tau_i,\tau_j)}$, the probability density function of S can be approximated as [38]

$$p\,(S) = \frac{1}{S\sigma_S\sqrt{2\pi}}\mathrm{e}^{-\frac{(\ln S-\mu_S)^2}{2\sigma_S^2}}\quad, \tag{A.3}$$

where

$$\begin{aligned}
\mu_S &= \ln\left(\mathbb{E}\left[S\right]\right) - \frac{1}{2}\ln\left(1+\frac{\mathbb{V}ar\left[S\right]}{\mathbb{E}\left[S\right]^2}\right)\\
\sigma_S &= \sqrt{\ln\left(1+\frac{\mathbb{V}ar\left[S\right]}{\mathbb{E}\left[S\right]^2}\right)}\\
\mathbb{E}\left[S\right] &= \begin{bmatrix} c_1 & c_2 & \cdots & c_n\end{bmatrix}\begin{bmatrix}\mu_{\tau_1}\\ \mu_{\tau_2}\\ \vdots\\ \mu_{\tau_n}\end{bmatrix}\\
\mathbb{V}ar\left[S\right] &= \begin{bmatrix} c_1 & c_2 & \cdots & c_n\end{bmatrix}\begin{bmatrix}\sigma^2_{\tau_1} & \sigma_{(\tau_1,\tau_2)} & \cdots & \sigma_{(\tau_1,\tau_n)}\\ \sigma_{(\tau_2,\tau_1)} & \sigma^2_{\tau_2} & \cdots & \sigma_{(\tau_2,\tau_n)}\\ \vdots & \vdots & \ddots & \vdots\\ \sigma_{(\tau_n,\tau_1)} & \sigma_{(\tau_n,\tau_2)} & \cdots & \sigma^2_{\tau_n}\end{bmatrix}\begin{bmatrix}c_1\\ c_2\\ \vdots\\ c_n\end{bmatrix}.
\end{aligned} \tag{A.4}$$

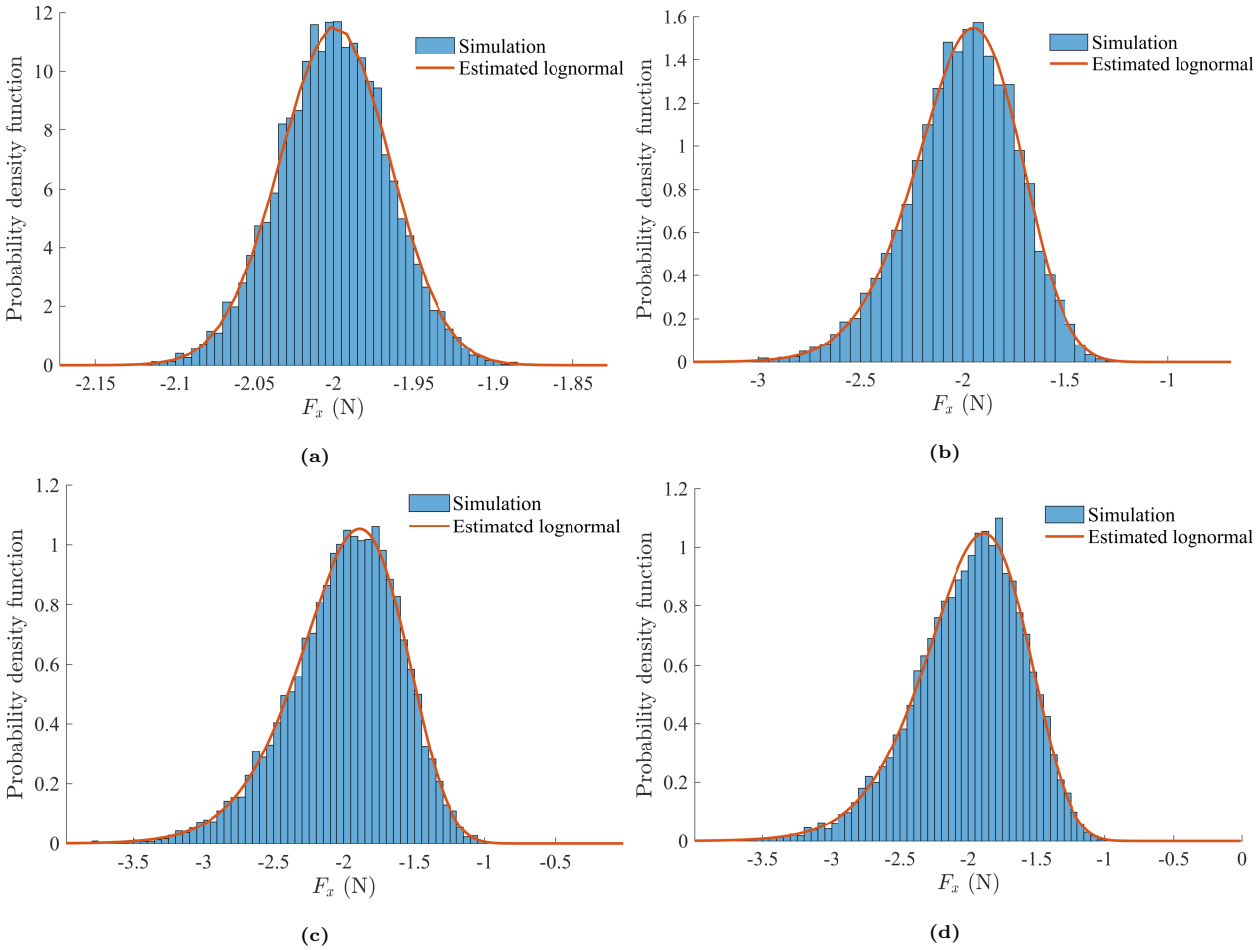

Fig. A.1. Simulation of F_x and estimated lognormal distribution. (a) $l/a = 0.1$; (b) $l/a = 1$; (c) $l/a = 10$; (d) $l/a = 100$.

Four realizations of F_x with different l/a ranging from 0.1 to 100 are presented in Fig.A.1. In each case, although the variances of the F_x are varied (the mean values stay the same), the estimated lognormal distributions capture the probability density quite well. For the random variable T_G, the situation is different from F_x because the positiveness of the coefficients (in this case $c_i = P\, y_i\, dS_i$) can not be guaranteed, which is due to the possible negativeness in the coordinate y_i. Bear in mind from Eq.8 that the mean value of T_G is 0, those negative coefficients may result in a negative summation, which means T_G certainly can not be of a lognormal distribution. However, if the geometry of the contact interface is symmetric (like in this case the square plate), in other words, the positive coefficients and negative coefficients are of the same amount, it is reasonable to assume their summation shows some "normality", and thus the statistical properties of T_G can be used to generate the corresponding estimated normal distribution. Four realizations of T_G with different l/a ranging from 0.1 to 100 are shown in Fig.A.2, in which the estimated normal distributions show good consistency with the simulated ones.

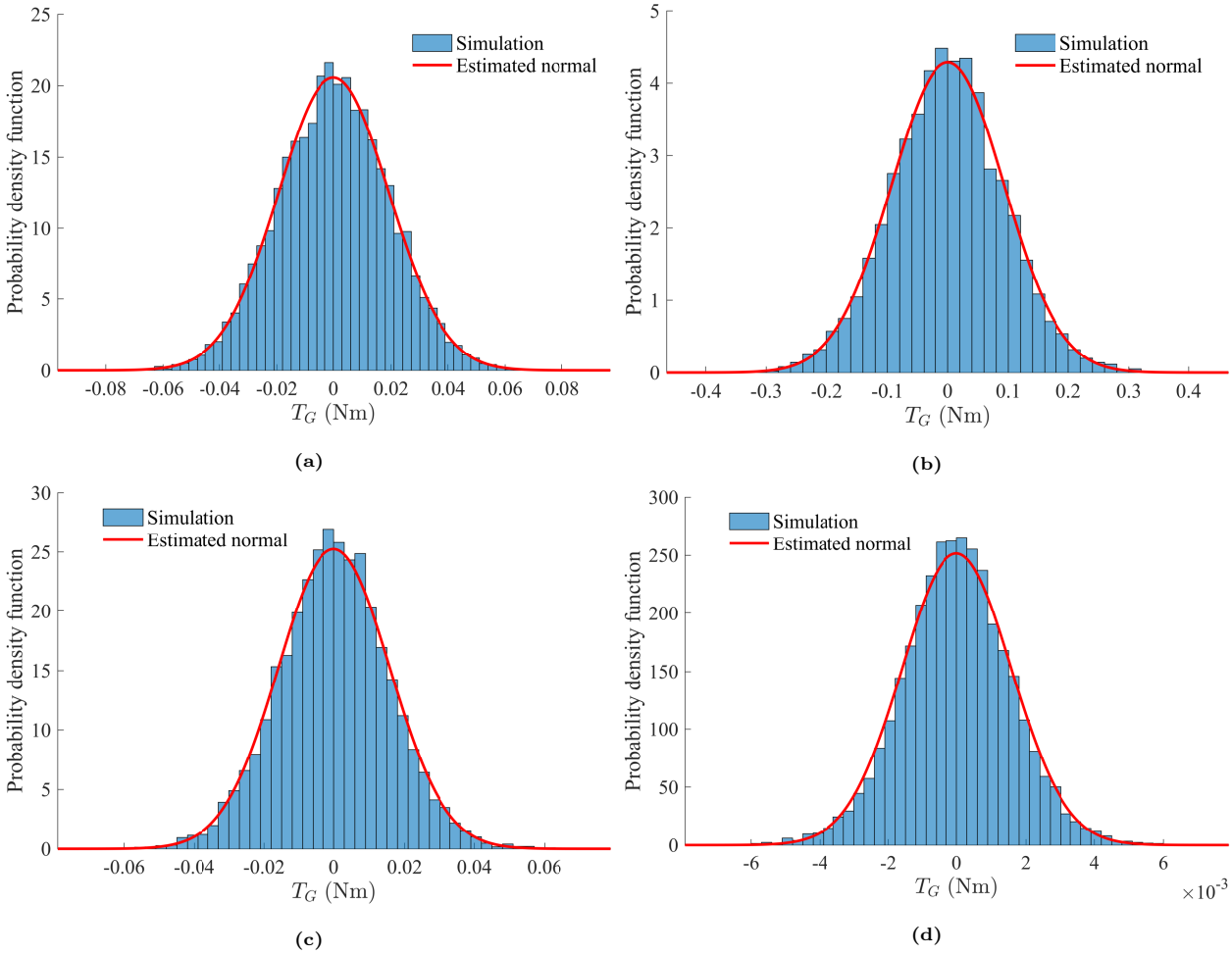

Fig. A.2. Simulation of T_G and estimated normal distribution. (a) $l/a = 0.1$; (b) $l/a = 1$; (c) $l/a = 10$; (d) $l/a = 100$.

Appendix B Crank-slider system equations of motion

The Lagrangian function L is defined as $L \equiv T - V$, in which T is the kinetic energy of the crank-slide system and V the potential energy as

$$\begin{aligned} T &= \frac{1}{2}J_1\dot{\theta}^2 + \frac{1}{2}J_2\dot{\phi}^2 + \frac{1}{2}m_2(\dot{x_2}^2 + \dot{y_2}^2) + \frac{1}{2}m_3\dot{x_3}^2 \\ &= \frac{1}{4}m_1R^2\dot{\theta}^2 + \frac{1}{6}m_2L^2\dot{\phi}^2 + \frac{1}{2}m_2R^2\dot{\theta}^2\sin^2\theta + \frac{1}{2}m_2RL\dot{\theta}\dot{\phi}\sin\theta\sin\phi \\ &+ \frac{1}{2}m_3R^2\dot{\theta}^2\sin^2\theta + m_3RL\dot{\theta}\dot{phi}\sin\theta\sin\phi + \frac{1}{2}m_3L^2\dot{\phi}^2\sin^2\phi \end{aligned} \tag{B.1}$$

$$V = m_2gy_2 = \frac{1}{2}m_2gLsin\phi \ , \tag{B.2}$$

where $J_1 = \frac{1}{2}m_1R^2$, $J_2 = \frac{1}{3}m_2L^2$. The constraint equation can be expressed as

$$\mathbf{\Phi(q)} = R\sin\theta - L\sin\phi = 0 \ , \tag{B.3}$$

then the generalized constraint reaction force can be derived as $\mathbf{Q}_C = \lambda\mathbf{\Phi_q}$, where λ is the Lagrange multiplier and $\Phi_q = \frac{\partial\mathbf{\Phi(q)}}{\partial\mathbf{q}} = [R\cos\theta, -L\sin\phi]^T$. The generalized force is obtained by using virtual work principle.

The virtual work δW done by external disturbance force and torque can be expressed as

$$\delta W = \kappa\delta\theta + (f_s + f_b)\delta x_3 = \mathbf{q}^T\mathbf{Q}_A \ , \tag{B.4}$$

where f_s and f_b are the friction forces of the side and bottom of the slider-track contact interface, which can be derived through Eq.4, Eq.5 and Eq.32. The normal pressure P in the equations should be computed by $P = F_n/S$, where $S = 4a^2$ and F_n is the normal force of the slider that can be derived iteratively through Eq.B.5.

$$\begin{aligned} F_n = -\frac{1}{12}\big[&3m_2RL\sin\theta\cos\phi^2\dot{\phi}^2 - 6m_2RL\cos\theta\cos\phi^2\dot{\phi}^2 + 3m_2RL\cos\phi\cos\theta\sin\phi\dot{\phi}^2 \\ &- 6m_2R^2\cos\theta\sin\theta\sin\phi\dot{\phi}^2 + 3m_2RL\sin\theta\sin\phi\cos\phi\ddot{\phi} - 3m_2RL\cos\phi^2\cos\theta\ddot{\phi} \\ &- 6m_2RL\cos\theta\sin\phi\cos\phi\ddot{\phi} + 6m_2R^2\cos\theta^2\sin\phi\ddot{\theta} - 3m_2RL\sin\theta\dot{\phi}^2 \\ &+ 6m_2RL\cos\theta\dot{\phi}^2 + m_2RL\sin\theta\ddot{\phi} - 6m_2gR\cos\phi\cos\theta - 12m_2gR\cos\theta\sin\phi \\ &- 6m_2R^2\sin\phi\ddot{\theta} + 6m_1R^2\sin\phi\ddot{\theta} - 12\sin\phi\kappa]/[R(\sin\phi\cos\theta + \sin\theta\cos\phi)] + m_3g. \end{aligned} \tag{B.5}$$

Recall the Lagrange equations of the second kind

$$\frac{d}{d\mathbf{q}}(\frac{\partial L}{\partial\dot{\mathbf{q}}}) - \frac{\partial L}{\partial\mathbf{q}} + \mathbf{Q}_C = \mathbf{Q}_A \ , \tag{B.6}$$

the dynamic differential equations of the system are finally obtained as:

$$\mathbf{M}(\mathbf{q})\ddot{\mathbf{q}} + \mathbf{F}(\mathbf{q},\dot{\mathbf{q}}) + \mathbf{Q}_C = \mathbf{Q}_A \ , \tag{B.7}$$

where

$$\mathbf{M} = \begin{bmatrix} M_{11} & M_{12} \\ M_{21} & M_{22} \end{bmatrix}, \mathbf{F} = \begin{bmatrix} F_\theta \\ F_\phi \end{bmatrix}, \tag{B.8}$$

in which

$$\begin{aligned} M_{11} &= \frac{1}{2}m_1R^2 + (m_2+m_3)R^2\sin^2\theta \\ M_{22} &= \frac{1}{3}m_2L^2 + m_3L^2\sin^2\phi \\ M_{12} &= M_{21} = (\frac{1}{2}m_2 + m_3)RL\sin\theta\sin\phi \\ F_\theta &= (m_2+m_3)R^2\dot{\theta}^2\sin\theta\cos\theta + (\frac{1}{2}m_2+m_3)RL\dot{\phi}^2\sin\theta\cos\phi \\ F_\phi &= (\frac{1}{2}m_2+m_3)RL\dot{\theta}^2\cos\theta\sin\phi + m_3L^2\dot{\phi}^2\sin\phi\cos\phi + \frac{1}{2}m_2gL\cos\phi. \end{aligned} \tag{B.9}$$

References

[1] E. Pennestrì, V. Rossi, P. Salvini, P. P. Valentini, Review and comparison of dry friction force models, Nonlinear Dyn. 83 (4) (2016) 1785–1801. doi:https://doi.org/10.1007/s11071-015-2485-3.

[2] Q. Feng, A discrete model of a stochastic friction system, Comput. Methods Appl. Mech. Eng. 192 (20) (2003) 2339 – 2354. doi:https://doi.org/10.1016/S0045-7825(03)00241-X.

[3] C. Chevennement-Roux, T. Dreher, P. Alliot, E. Aubry, J. Lainé, L. Jézéquel, Flexible wiper system dynamic instabilities: Modelling and experimental validation, Exp. Mech. 47 (2007) 201–210. doi:10.1007/s11340-006-9027-3.

[4] E. Rabinowicz, Friction coefficients of noble metals over a range of loads, Wear 159 (1) (1992) 89–94.

[5] O. Ben-David, J. Fineberg, Static friction coefficient is not a material constant, Phys. Rev. Lett. 106 (25) (2011) 254301.

[6] A. Culla, F. Massi, Uncertainty model for contact instability prediction, J. Acoust. Soc. Am. 126 (3) (2009) 1111–1119. doi:https://doi.org/10.1121/1.3183376.

[7] A. R. Lima, C. F. Moukarzel, I. Grosse, T. J. P. Penna, Sliding blocks with random friction and absorbing random walks, Phys. Rev. E 61 (3) (2000) 2267–2271. doi:10.1103/physreve.61.2267. URL http://dx.doi.org/10.1103/PhysRevE.61.2267

[8] E. Sarrouy, O. Dessombz, J.-J. Sinou, Piecewise polynomial chaos expansion with an application to brake squeal of a linear brake system, J. Sound Vib. 332 (3) (2013) 577 – 594. doi:https://doi.org/10.1016/j.jsv.2012.09.009.

[9] L. Nechak, S. Berger, E. Aubry, Prediction of Random Self Friction-Induced Vibrations in Uncertain Dry Friction Systems Using a Multi-Element Generalized Polynomial Chaos Approach, J. Vib. Acoust. 134 (4). doi:10.1115/1.4006413.

[10] T. Ritto, M. Escalante, R. Sampaio, M. Rosales, Drill-string horizontal dynamics with uncertainty on the frictional force, J. Sound Vib. 332 (1) (2013) 145 – 153. doi:https://doi.org/10.1016/j.jsv.2012.08.007.

[11] W. S. Kang, C. K. Choi, H. H. Yoo, Stochastic modeling of friction force and vibration analysis of a mechanical system using the model, J. Mech. Sci. Technol. 29 (9) (2015) 3645–3652. doi:https://doi.org/10.1007/s12206-015-0808-4.

[12] A. Nobari, H. Ouyang, P. Bannister, Statistics of complex eigenvalues in friction-induced vibration, J. Sound Vib. 338 (2015) 169–183.

[13] C. Snoun, B. Bergeot, S. Berger, Prediction of the dynamic behavior of an uncertain friction system coupled to nonlinear energy sinks using a multi-element generalized polynomial chaos approach, Eur. J. Mech. A. Solids 80 (2020) 103917.

[14] B. Choi, M. Sipperley, M. Mignolet, C. Soize, Discrete maximum entropy process modeling of uncertain properties: Application to friction for stick-slip and microslip response, in: Proceedings of the 8th International Conference on Structural Dynamics, EURODYN 2011, University of Southampton, Institute of Sound Vibration and Research, 2011, pp. 2626–2633, 8th International Conference on Structural Dynamics, EURODYN 2011 ; Conference date: 04-07-2011 Through 06-07-2011.

[15] S. Qiao, D. Beloiu, R. Ibrahim, Deterministic and stochastic characterization of friction-induced vibration in disc brakes, Nonlinear Dyn. 36 (2-4) (2004) 361–378.

[16] E. Gravanis, L. Pantelidis, D. Griffiths, An analytical solution in probabilistic rock slope stability assessment based on random fields, Int. J. Rock Mech. Min. Sci. 71 (2014) 19–24.

[17] X. Zhou, Y. Xie, X. Huang, B. Zhu, Probabilistic analysis of step-shaped slopes using random field models, Int. J. Geomech. 20 (1) (2020) 04019145.

[18] X. Huang, X. Zhou, W. Ma, Y. Niu, Y. Wang, Two-dimensional stability assessment of rock slopes based on random field, Int. J. Geomech. 17 (7) (2017) 04016155.

[19] X.-P. Zhou, B.-Z. Zhu, C.-H. Juang, L. N. Y. Wong, A stability analysis of a layered-soil slope based on random field, Bull. Eng. Geol. Environ. 78 (4) (2019) 2611–2625.

[20] A. A. Kireenkov, S. V. Ramodanov, Combined dry friction models in the case of random distribution of the normal contact stresses inside contact patches, in: COUPLED VIII: proceedings of the VIII International Conference on Computational Methods for Coupled Problems in Science and Engineering, CIMNE, 2019, pp. 176–182.

[21] K. Wierzcholski, Determination of random friction forces on the biological surfaces of a human hip joint with a phospholipid bilayer, Tribologia.

[22] K. Wierzcholski, A. Miszczak, Estimation of random friction forces on the microbearing cooperating surfaces, Journal of KONES 26 (2) (2019) 167–174.

[23] A. V. Borisov, I. S. Mamaev, N. N. Erdakova, Dynamics of a body sliding on a rough plane and supported at three points, Theor. Appl. Mech. Lett. 43 (2) (2016) 169–190. doi:https://doi.org/10.2298/TAM161130013B.

[24] S. Goyal, A. Ruina, J. Papadopoulos, Planar sliding with dry friction part 2. dynamics of motion, Wear 143 (2) (1991) 331 – 352. doi:https://doi.org/10.1016/0043-1648(91)90105-4.

[25] J. Zhou, R. Paolini, J. A. Bagnell, M. T. Mason, A convex polynomial force-motion model for planar sliding: Identification and application, in: 2016 IEEE International Conference on Robotics and Automation (ICRA), IEEE, 2016, pp. 372–377.

[26] M. M. Ghazaei Ardakani, J. Bimbo, D. Prattichizzo, Quasi-static analysis of planar sliding using friction patches, Int. J. Rob. Res. 39 (14) (2020) 1775–1795.

[27] A. Or, The dynamics of a tippe top, SIAM J. Appl. Math. 54 (3) (1994) 597–609.

[28] A. A. Kilin, E. N. Pivovarova, Conservation laws for a spherical top on a plane with friction, Int. J. Non Linear Mech. (2020) 103666.

[29] V. P. Zhuravlev, D. Klimov, Global motion of the celt, Mech. Solids 43 (3) (2008) 320–327.

[30] A. Kireenkov, Combined model of sliding and rolling friction in dynamics of bodies on a rough plane, Mech. Solids 43 (3) (2008) 412–425.

[31] F. Chen, M. Abdelhamid, P. Blaschke, J. Swayze, On automotive disc brake squeal part iii test and evaluation, in: SAE 2003 Noise and Vibration Conference and Exhibition, SAE International, 2003. doi:https://doi.org/10.4271/2003-01-1622.

[32] L. C. Andrews, Special functions of mathematics for engineers, Vol. 49, Spie Press, 1998.

[33] A. D. Kiureghian, J.-B. Ke, The stochastic finite element method in structural reliability, Probab. Eng. Mech. 3 (2) (1988) 83 – 91. doi:https://doi.org/10.1016/0266-8920(88)90019-7.

[34] Y. Liu, J. Li, S. Sun, B. Yu, Advances in gaussian random field generation: a review, Comput. Geosci. (2019) 1–37doi:https://doi.org/10.1007/s10596-019-09867-y.

[35] A. Batou, T. Ritto, R. Sampaio, Entropy propagation analysis in stochastic structural dynamics: application to a beam with uncertain cross sectional area, Comput. Mech. 54 (3) (2014) 591–601. doi:https://doi.org/10.1007/s00466-014-1008-2.

[36] P.-L. Liu, A. Der Kiureghian, Multivariate distribution models with prescribed marginals and covariances, Probab. Eng. Mech. 1 (2) (1986) 105–112.

[37] N. C. Beaulieu, An extended limit theorem for correlated lognormal sums, IEEE Trans. Commun. 60 (1) (2011) 23–26.

[38] C. Rook, M. Kerman, Approximating the sum of correlated lognormals: An implementation, Available at SSRN 2653337.